Journal of Industrial and Engineering Chemistry xxx (xxxx) xxx

Contents lists available at ScienceDirect

Journal of Industrial and Engineering Chemistry

journal homepage: www.elsevier.com/locate/jiec

Improvement of the flame retardancy of polyamide 6 by the incorporation of UiO-66 and UiO-66/melamine

Cristina Pina-Vidal [a,b], Víctor Berned-Samatán [a,b], Elena Piera [c], Miguel A. Caballero [c], Carlos Téllez [a,b,*]

[a] Instituto de Nanociencia y Materiales de Aragón (INMA) CSIC-Universidad de Zaragoza, 50018 Zaragoza, Spain
[b] Chemical and Environmental Engineering Department, Universidad de Zaragoza, 50018 Zaragoza, Spain
[c] Research and Development Department. Nurel S.A., Ctra. Barcelona km 329, 50016 Zaragoza, Spain

ARTICLE INFO

Keywords:
Flame retardant
Polyamide
UiO-66
Melamine
UL-94
LOI

ABSTRACT

The flame retardancy of polyamide 6 (PA6) has been investigated through the incorporation of the metal–organic framework (MOF) UiO-66 and a composite of UiO-66/melamine during the extrusion process. The prepared materials have been characterised by various techniques: XRD, XPS, FTIR, TGA, DSC, SEM, EDX and mechanical properties. Moreover, to examine the efficiency of the flame retardants, the composites have been tested using the UL-94 vertical and, horizontal burning test, as well as the limiting oxygen index (LOI). The UL-94 V-2 standard has been achieved with only a 4 wt% load of either UiO-66 or UiO-66/melamine, compared to pure polyamide, which is not classified. The best results have been achieved with the UiO-66/melamine sample at 7 wt%, which prevents the agglomeration of UiO-66 alone. The highest LOI value was also obtained with this sample, achieving a value of 35.5 %, compared to pure PA6 and with UiO-66, which reached values of 22.4 % and 23.2 %, respectively. A flame suppression mechanism of the UiO-66/melamine composite is proposed, based on the formation of zirconium oxide, gas adsorption by the MOF and release of NH_3.

Introduction

The use of polymers is becoming more and more widespread in several applications, including electronic and electrical products, materials used in transport vehicles, building-construction materials, high-performance hardware manufacturing, and upholstery, among others. The potential fires caused by polymers can have devastating consequences. It is therefore, essential to develop of flame retardant materials, which can be incorporated into the fabrication of these polymers, to reduce the risk of fire. Polyamide 6 (PA6) is one of the most important engineering plastics, widely used in many industrial applications [1,2] due to its chemical stability, as well as its excellent mechanical and electrical characteristics (see structure in Fig. 1a). Such applications range from clothing fibres to automotive components. The combustion of PA6 releases high heat, and toxic gases, and there is also a noticeable polymer dripping that leads to a very fast flame propagation [3]. For this reason, certain sectors require PA6 to possess flame retardant properties in addition to its inherent qualities. However, this material is susceptible to burning due to its low limiting oxygen index (around 23 % [4]). Therefore, addressing how to provide PA6 with flame-retarding properties has emerged as a crucial area of research [5].

Traditionally, halogen-containing flame retardants are the most widely used due to their high efficiency. However, they present some disadvantages, such as the volatilization of toxic gases and the corrosion of metal components during combustion. Consequently, the regulations concerning these materials are becoming more stringent or their use is even forbidden. For this reason, there has been a growing interest in halogen-free flame retardants in recent years.

Metal-organic frameworks (MOFs) are a promising class of crystalline porous materials with unique properties. These compounds are

Abbreviations: BDC, benzenedicarboxylic acid; BET, Brunauer-Emmett-Teller; COF, covalent organic frameworks; DSC, differential scanning calorimetry; EDX, energy dispersive X-ray; EtOH, ethanol; fcu, face centered cubic; FTIR, Fourier transform infrared spectroscopy; hcp, hexagonal closed packed; LOI, limiting oxygen index; MOF, metal-organic frameworks; NR, not rated; PA6, polyamide 6; SEM, scanning electron microscopy; TEABr, tetraethylammonium bromide; TEM, transmission electron microscopy; TGA, thermogravimetric analysis; UiO-66, University of Oslo 66; UL-94, Underwriters Laboratories 94; XPS, X-ray photoelectron spectroscopy; XRD, X-ray diffraction.

* Corresponding author at: Instituto de Nanociencia y Materiales de Aragón (INMA) CSIC-Universidad de Zaragoza, 50018 Zaragoza, Spain.
E-mail address: ctellez@unizar.es (C. Téllez).

https://doi.org/10.1016/j.jiec.2024.10.026
Received 15 July 2024; Received in revised form 24 September 2024; Accepted 11 October 2024
Available online 18 October 2024

essentially formed by connecting metal ions or clusters with organic linkers through coordination bonds. Due to their exceptionally high specific surface area, tunable pore size distribution, and high thermal and chemical stability, MOFs receive notable interest in the areas of gas [6] and energy storage [7], gas separation [8], catalysis [9–13], luminescence [14], adsorbents for environmental water [15], and encapsulation for drug [16] or cosmetic [17] release. In addition, these materials emerge as a new class of additives that reduce fire hazards in polymeric materials. Due to their inorganic–organic hybrid nature, MOFs are usually more compatible with polymers to form polymer composites. Furthermore, in terms of sustainability, MOFs can be recovered from their mixture with polymers by dissolving the latter in order to reuse the MOF [18]. These composites have shown promising flame retardant properties and great thermal stability [19,20], which can be attributed to their chemical composition. As a consequence of the thermal decomposition, MOFs form metal oxides, which cover the surface of the polymer. This layer can serve as an insulating physical barrier against further burning, as it limits the exposure of the polymer surface to air [21], and efficiently adsorbs the gases and smoke [22]. It will therefore reduce the accessible fuel for further combustion and the heat release [23,24].

Zr-based MOFs attract much attention due to their exceptional chemical, mechanical, thermal, and structural stability, which are attributed to the high number of coordination of these MOFs [25]. Thus, they show better stability against shear stress than other types of MOFs. In addition, it is known that the MOFs synthesised with transition metal elements such as zirconium can catalyse the char formation reactions at high temperatures [26]. Moreover, their high specific surface area due to the large number of pores can be useful for the adsorption of pyrolysis gases. UiO-66 (University of Oslo 66) is made up by the coordination reaction of $Zr_6O_4(OH)_4$ clusters and 1,4-benzodicarboxylic acid (BDC) (Fig. 1b). This MOF is useful in smoke suppression, as demonstrated in polystyrene [27]. Some authors have improved the flame retardancy and thermal stability by incorporating 4 % UiO-66 into polycarbonate [28]. The functionalized form, UiO-66-NH_2, combined with a phosphate additive has also been used in polylactic acid polymer [29] and in polyester [30] as a flame retardant. Similarly, a hybrid of UiO-66 with Prussian blue analogues and polydopamine has been used to improve the fire retardancy and smoke suppression properties of an epoxy polymer [31]. Therefore, given its exceptional thermal stability compared to other MOFs, UiO-66 can be introduced at the extrusion temperatures of PA6 (ca. 260 °C) in order to test the capacity as a flame retardant that is has shown in other polymers.

Recently, nitrogen-containing compounds have received more attention in flame retardant applications. Melamine is a triazine compound with a high nitrogen content (Fig. 1c), commonly used as a flame retardant additive due to its low cost and non-toxicity after combustion. The thermal decomposition of melamine can produce inert gases such as NH_3, which dilute the combustible gases [3,32]. Moreover, the condensation of melamine produces melem, melam and melon, which are considered flame retardant compositions due to their exceptional thermal stability and decomposition properties [33]. Melamine and its salts (melamine cyanurate) have been extensively used in flame retardancy, achieving great results [34,35]. The following compounds can be used in combination with other additives to improve the mechanical strength and thermal stability of the polymer, as well as its flame retardancy: melamine/cloisite in Pebax [36], melamine/melamine phosphate/zirconium phosphate in polypropylene [37] and melamine cyanurate/zirconium phosphate [38]. Additionally, melamine has been combined with MOFs for heavy metal removal applications, such as Co (II) [39] and Pb (II) [40]. It has also been tested in combination with covalent organic frameworks (COFs) for CO_2/CH_4 separation [41]. Consequently, the combination of UiO-66 and melamine may be of great interest for the development of modified flame retardants.

In this work, different flame retardant materials have been tested. First, UiO-66 was synthesised using a solvent-free method, which is easily scalable and can produce several grams of product. Two samples were prepared from this procedure: one properly washed and activated at a high temperature and the other barely washed and activated at a lower temperature, to check if the process could be more sustainable. Besides, a novel hybrid of melamine and UiO-66 was prepared to improve flame retardant efficiency. A new synthesis of this material (UiO-66/melamine) was conducted following the same method used for UiO-66, but replacing the template (TEABr) with melamine in the synthesis media. Furthermore, the sample was barely washed and not activated, which made its preparation more sustainable. To our knowledge, this was the first time that UiO-66 samples and a UiO-66/melamine composite were incorporated into PA6 by injection moulding, obtaining composites with different additive loads (from 1 % to 7 %). The flame retardancy of the prepared PA6 composites was determined using the UL-94 vertical and horizontal burning test and limiting oxygen index (LOI). These tests assess the flame retardancy degree and dripping behaviour. In addition, the mechanical properties were determined to know the influence of flame retardants in the composites.

Materials and methods

Materials

Zirconium (IV) oxychloride octahydrate ($ZrOCl_2{\cdot}8H_2O$, Glentham Life Sciences, 98 %) and tetraethylammonium bromide (TEABr, TCI chemicals, >98 %) were supplied by CymitQuimica. 1,4-benzenedicarboxylic acid (BDC, Aldrich, 98 %) and melamine (Acros Organics, 99 %) were purchased from Sigma-Aldrich. Ethanol (EtOH, 96 %), as cleaning solvent, was provided by Productos Gilca S.C. Polyamide (PA6), injection moulding grade, was provided by Nurel S.A.

Synthesis of flame retardant materials

The preparation of UiO-66 was carried out following an efficient solvent-free method, which is described in literature [17]. The synthetic procedure was conducted as follows: a physical mixture of $ZrOCl_2{\cdot}8H_2O$

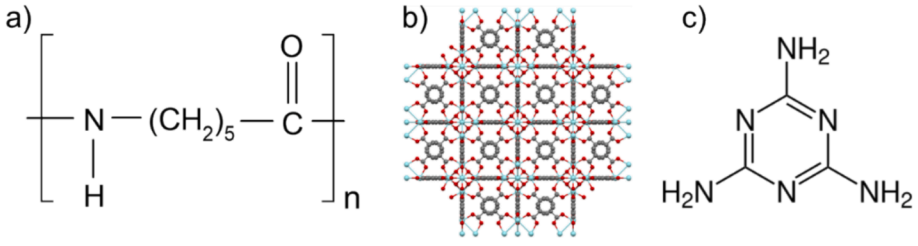

Fig. 1. Molecular structure of the main materials used in this work a) PA6, b) UiO-66 and, c) Melamine. The structures of PA6 and melamine have been drawn with ChemSketch software [42]. The representation of UiO-66 is made using Mercury 3.8 software [43]. CIF file was obtained from the Cambridge Crystallographic Data Centre (CCDC 1018045) [44]. (Oxygen in red, carbon in grey and zirconium in light blue).

(100 mmol, 32.2 g), BDC (100 mmol. 16.6 g) and TEABr (142 mmol, 29.8 g) was ground in a mortar for about 10 min until it had an homogenous appearance. Then, it was transferred to an autoclave and left at 190 °C for 24 h. Afterwards, the autoclave was cooled down and the resulting solid was washed with warm ethanol (three or four times). Next, the solid was placed in a vacuum oven at 200 °C during 12 h for the MOF activation. In order to obtain a porous framework free of unreacted ligand, the solid was calcined in an oven at 250 °C for 4 h with a heating ramp of 2 °C/min. Therefore, this method produced properly activated UiO-66. Another UiO-66 sample was prepared with less activation after the synthesis. Once the solid was removed from the autoclave, it was washed only once with ethanol. Then, it was dried at 100 °C in order to eliminate the solvent inside the pores.

The incorporation of melamine into the synthesis was carried out following a similar method to the one described above. It consisted of replacing the structural template (TEABr) used in the UiO-66 synthesis with melamine. Therefore, the procedure involved grinding a physical mixture of $ZrOCl_2 \cdot 8H_2O$ (100 mmol, 32.2 g), BDC (100 mmol, 16.6 g) and melamine (30 mmol, 3.78 g) in a mortar. The homogeneous solid was transferred to an autoclave and left at 190 °C for 24 h. The resulting solid was washed once with ethanol to avoid removing the melamine. Afterwards, the solid was dried overnight at 100 °C to remove the solvent. The resulting solid will be called UiO-66/melamine.

Preparation of composites

The polyamide was premixed with the flame retardant solids and this mixture was melted at a temperature of 260 °C using an Arbug 320C injection moulding machine, to prepare the polymeric composite specimens according to UNE-EN ISO 294-1. The weight of polymer required to prepare the polymeric specimens was 500 g. Therefore, for the tested load percentages 1, 2, 4, and 7 %, the amount of flame retardant samples added to the polymer was 5, 10, 20, and 35 g, respectively. Fig. 2 shows images of the prepared samples at different percentages of flame retardant loads. The PA6 sample presented a whitish appearance. The composites with flame retardant showed a uniform appearance and a good distribution of the solids, without the formation of aggregates. However, it was observed that the higher the load percentage, the more yellowish they became. This observation was particularly true for the non-activated UiO-66 composites, likely due to the fact that this sample was not washed properly and may have contained unreacted ligand and structural agent.

Flame retardant tests

Vertical and horizontal burning test methods (UL-94)

The vertical burning test (UL-94 V) was conducted using a custom experimental setup designed for this purpose. This experiment is approved by "Underwriters' Laboratories" to assess the flammability of plastic materials intended for use in devices and appliances. The sample dimensions were 125 mm × 13 mm × 1.5 mm. Fig. 3a shows a schematic representation of the experimental setup used in the UL-94 V test. This method consisted of burning an end of the sample for 10 s and recording the time it took for the flame to extinguish. A second flame was then applied for 10 s, and the extinguishing time was measured again. The dripping behaviour after flame exposure was also analysed. A piece of cotton, which could ignite due to the polymeric drops released from the specimen, was placed below the sample. The UL-94 V test categorized the materials as V0, V1, V2 or NR (not rated) and assessed the dripping features of the samples according to UNE-EN 60695-11-10. A V0 classification indicated that the flame in the sample extinguishes quickly, representing the highest rating. And NR is when it does not meet the conditions of V0, V1 and V2 to be classified, and it is necessary to perform the horizontal burning test to assess the flammability of the samples. Classification criteria for this test are detailed in Table S1.

The horizontal combustion test (Fig. 3b) was also performed on the samples with the highest load of flame retardants (7 wt%) to determine the linear combustion rate of the polymeric composites. This value is calculated, in millimetres per minute, for each sample in which the flame travels from the 25 mm mark to the 100 mm mark.

Limiting oxygen index (LOI)

This combustion test provides information about the minimum concentration of oxygen that is needed to support the combustion of a material. This test was carried out for activated UiO-66 and UiO-66/melamine samples with a load of 7 wt%. The dimensions of the specimens are 125 mm × 13 mm × 1.5 mm. This test was performed according to standard rule UNE-EN ISO 4589-2:2017.

Mechanical properties

The influence of the incorporation of flame retardant samples on the mechanical properties was tested by measuring the following mechanical parameters:

- Tensile properties (according to ISO 527-1/-2). This test provides important data such as tensile modulus, elongation at break and tensile strength. These properties help to determine the material's

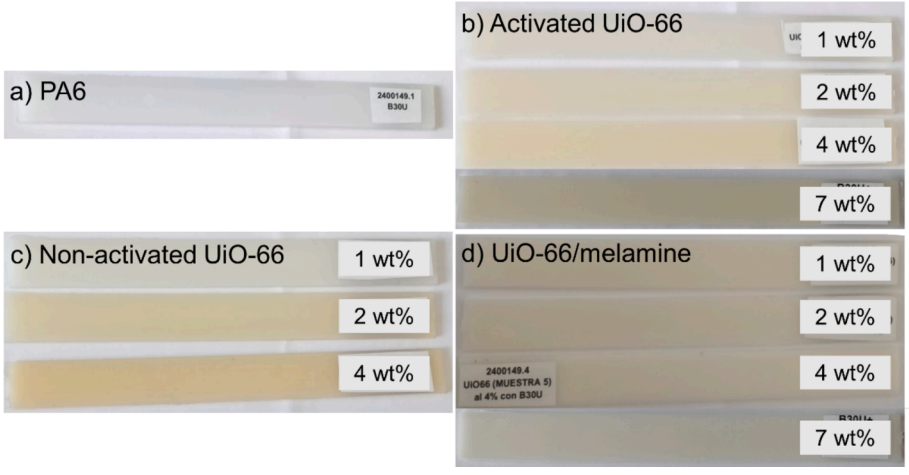

Fig. 2. Photographs of the polyamide 6 (PA6) composites used in the flame retardant test a) PA6, b) PA6 + activated UiO-66, c) PA6 + non-activated UiO-66 and d) PA6 + UiO-66/melamine.

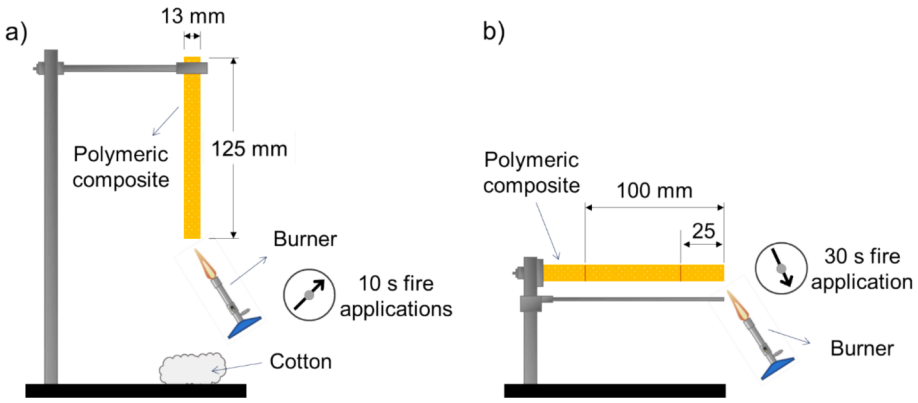

Fig. 3. Experimental setup used in the a) UL-94 V test and b) Horizontal combustion test for flame retardancy evaluation.

performance under load. The specimen is usually a "dumbbell-shaped" sample with standardised dimensions (4 mm × 150 mm total length × 20 mm (central part 80 mm × 10 mm)). This test is carried out on a universal testing machine (INSTRON 3367 Serie dual column 30kN table model), which grips the two ends of the specimen and pulls them apart at a constant speed, applying a uniaxial tensile force. It was performed at 23 °C using a traction speed of 1 mm/min for the tensile modulus and a value of 50 mm/min for the rest of measurements.

- Charpy notched impact strength (according to ISO 179/1eA). This test was performed at 23 °C. The dimensions of the specimen were 4 mm × 10 mm × 80 mm (with a notch in the middle). It was placed horizontally and a heavy pendulum hammer was released from a known height, swinging downwards and striking the non-notched side of the specimen, causing it to break. The energy required to break it was absorbed by the pendulum's kinetic energy. The machine records the difference in the pendulum's potential energy, which indicates how much energy was absorbed during the fracture. The impact resistance was calculated by dividing the impact energy in kJ by the area under the notch.
- Heat deflection temperature (HDT) (according to ISO 75-1/-2). This test is used to measure the temperature at which a material begins to deform under a specified load. It helps to determine how well a material can withstand elevated temperatures without losing its shape. The specimen is usually a rectangular bar (4 mm × 10 mm × 80 mm) placed horizontally on supports separated by 100 mm. A constant load (in this case 1.8 MPa) was applied to the middle of the specimen. It was gradually heated at a controlled rate, typically 2 °C/min. The test records the temperature at which the specimen undergoes a deflection of 0.2 mm. This temperature is called 'heat deflection temperature'.

Characterization

X-ray diffraction (XRD) analysis was used to confirm the formation of UiO-66 and its presence in the composites. This analysis was performed in an Empyrean PANalytical diffractometer (Malvern Panalytical). Measurements were carried out with a scanning rate of 0.01°/s and data were collected in the 2θ range of 2.5-40°. It was equipped with a copper anode and a graphite monochromator to select CuKα radiation (λ = 1.5406 Å).

Thermogravimetric analysis (TGA) was carried out on samples placed in 70 μL alumina pans using Mettler Toledo TGA/SDTA 854e equipment. A heating rate of 10 °C/min was used ranging from ambient temperature up to 700 °C under air atmosphere.

The thermal properties of the materials were characterized by differential scanning calorimetry (DSC). This analysis was performed on the polymeric composites in a Mettler Toledo DSC822e. Samples were subjected to an initial heating from 25 to 240 °C, and the cooled down to 25 °C. After that, they were heated up again to 600 °C, all at a heating rate of 10 °C/min. Samples were sealed in 100 μL aluminium crucibles with covers using a press. The degree of crystallinity (X_c) of the composites was calculated by: [34]

$$X_c = \frac{\Delta H_m}{(1-w) \bullet \Delta H_m^0} \bullet 100\% \quad (1)$$

where ΔH_m is the measured melting heat, ΔH_m^0 is the heat required to melt 100 % crystalline PA6 (191 J/g) [45] and w is the weight fraction of flame retardant incorporated in the polymer matrix.

Attenuated total reflection-Fourier transformed infrared spectroscopy (ATR-FTIR) was performed in a spectrometer (Bruker Vertex 70 FTIR) with a DTGS detector and a Golden Gate diamond ATR accessory. The spectra were recorded by averaging 40 scans in the 600–4000 cm^{-1} wavenumber range with a resolution of 4 cm^{-1}.

The chemical structures of the PA6 composites with flame retardant samples were determined by XPS using an AXIS Ultra DLD system from Kratos Analytical with a monochromatic Al Kα source (1486.6 eV) at 15 kV, 10 mA, and a power of 150 W. The XPS spectra were analysed using CasaXPS software.

To study the surface morphology of the samples, scanning electron microscopy (SEM) images were taken using an FEI-Inspect F50 microscope at an acceleration voltage of 10 kV. The samples were previously coated with palladium under vacuum conditions. In addition, compositional analysis was conducted performing an energy dispersive X-ray (EDX) analysis on the polymer composites to confirm the presence of UiO-66 inside them and determine the atomic percentage in different points of the sample. The polymer samples were cryogenically fractured under liquid nitrogen atmosphere to see and analyse their cross sections by electron microscopy. The particle size was measured from these images using ImageJ software.

The powder samples were analysed by Transmission Electron Microscopy (TEM) using a FEI Tecnai T20 microscope with an accelerating voltage of 200 kV. The samples were dispersed in ethanol and one drop of the solution was deposited on a carbon-coated grid.

A nitrogen adsorption analysis was performed to determine the textural properties of the samples. The Brunauer-Emmett-Teller (BET) method was used to measure specific surface areas and pore volumes, using a Micromeritics TriStar 3000 with previous degasification at 200 °C for 10 h in a Micromeritics VacPrep™ 061. The heating rate was 10 °C/min.

Results and discussion

Flame retardants characterization

The XRD spectra of UiO-66 and UiO-66/melamine samples are

shown in Fig. 4a. As can be seen in this graph, the UiO-66 sample exhibits the characteristic diffraction peaks at 2θ = 7.4°, 8.5° and 25.7° of the face centred cubic (fcu) crystal structure of UiO-66, corresponding to the crystallographic planes (111), (200) and (224), respectively [46]. These peaks seem to be more amorphous than the UiO-66 pattern, indicating its low crystallinity. In the case of the non-activated UiO-66 sample, the main peaks of BDC ligand also appear at 2θ = 17.4° and 28.0°. The sample with melamine shows typical peaks of another crystalline phase of UiO-66, in particular the hexagonal closed packed (hcp) structure. The characteristic peaks appear at 2θ = 4.7° [(002) plane], 7° [(100) plane] and 7.3° [(101) plane] [47]. This phase has been reported in the literature and it seems to be less thermally stable [48]. The pioneering authors of this structure have studied that the addition of ionic liquids (ILs) as a solvent seems to promote the formation of this crystalline phase [47,49]. Additionally, this sample exhibits some peaks related to melamine (29.8°) and BDC (17.4°, 25.2° and 28.0°), indicating that both melamine and unreacted ligand remain in the sample. This is because the sample was washed only once with ethanol to avoid removing melamine. According to the bibliography, if the synthesis is carried out without the template (TEABr), the sample obtained is not properly formed [50], presenting broader peaks, especially the main peaks of UiO-66 at 2θ = 7.4° and 8.5°. As with ILs, the presence of melamine seems to direct the formation of UiO-66 towards the hcp structure.

The textural properties of the flame retardant samples were also analysed and characterised by nitrogen adsorption–desorption. The main results are presented in Table 1 and Fig. 4b.

For UiO-66 samples (activated and non-activated), the isotherms are a combination of type I and type IV, suggesting the presence of micropores and mesopores. As expected, the BET surface area for the non-activated sample (379 m^2/g) is significantly lower than that of the activated UiO-66 (653 m^2/g). This decrease (42 %) is related to the presence of solvents and unreacted reactants inside the pores. The reported values of UiO-66 range from 600–1800 m^2/g [51], which are higher than the obtained value (653 m^2/g), indicating the lower crystallinity of the synthesised MOF, which is in agreement with the XRD results (Fig. 4a). In the case of the UiO-66 sample with melamine, it presents a very low BET surface area with a decrease of 91 %. This can be due to the presence of solvents and unreacted ligand, as well as the melamine filling the pores of UiO-66. Likewise, melamine and BDC, both detected by XRD, are not porous materials; therefore, non-encapsulated melamine and BDC do not contribute to surface area values. The variations in the total and microporous pore volume are consistent with what was previously mentioned about the specific surface area. The percentage decrease in the total pore volume and micropore volume in the non-activated sample is 42 % in both parameters, while in the sample with melamine these values decrease drastically to 88–93 %.

Table 1
Textural properties of UiO-66 samples and UiO-66/melamine. Decrease is calculated as ($Value_{activated}$-Value)/ ($Value_{activated}$)*100.

	BET Surface Area (m^2/g) / Decrease	Total Pore Volume[1] (cm^3/g) / Decrease	Micropore Volume[2] (cm^3/g) / Decrease
Activated UiO-66	653 ± 9 / 0 %	0.597 / 0 %	0.207 / 0 %
Non-activated UiO-66	379 ± 5 / 42.0 %	0.345 / 42.2 %	0.119 / 42.5 %
UiO-66/melamine	61 ± 1 / 90.7 %	0.04 / 93.3 %	0.024 / 88.4 %

[1] At $p/p^0 = 0.97$.
[2] Using t-plot.

The FTIR analysis of flame retardant materials (activated UiO-66, non-activated UiO-66 and UiO-66/melamine) was performed, and the resulting spectra are shown in Fig. 5. These samples were compared with each other and with melamine and BDC spectra to confirm the MOF synthesis and identify the main molecular groups. The FTIR spectrum of activated UiO-66 presents the main peaks of this MOF according to bibliography [17]. It displays a band at 1705 cm^{-1}, which is attributed to C=O stretching in non-dissociated acid groups [52]. The band at 1578 cm^{-1} is related to the carbonyl bond stretching vibration (C=O) of the carboxyl group. The small peak at 1507 cm^{-1} corresponds to the C=C vibration of the benzene ring. There is also a strong band at 1391 cm^{-1}, which is attributed to the C-O bond of the C-OH group of the carboxylic acid [53]. Additional characteristic bands for UiO-66 are observed at 743 and 653 cm^{-1} for the symmetric and asymmetric stretching of the O-Zr-O bonds, respectively [54]. While the FTIR spectrum of melamine show its main absorption peaks at 3468, 3415, 3322 and 3120 cm^{-1}, related to the stretching vibration of the primary amine (NH_2), the peaks at 1646, 1526 and 810 cm^{-1} are attributed to the triazine ring [55,56]. In the case of BDC spectra the peak at 1673 cm^{-1} corresponds to the C=O stretching of the carboxyl group. In addition, the peaks at 1423 and 927 cm^{-1} are related to the O–H bending vibrations of the carboxyl (COOH) group [57], and the strong peak at 1281 cm^{-1} is attributed to the C-O bond of the carboxylic acid [58]. In the non-activated sample, there are some small peaks related to BDC at 1281 and 927 cm^{-1}, as this sample was less washed and activated at a lower temperature. In the UiO-66/melamine sample, there are some peaks of melamine, such as the band at 3120 cm^{-1} related to the amine group. Moreover, this sample presents various peaks corresponding to the BDC linker, particularly the peaks at 1673, 1423 and 927 cm^{-1}. In

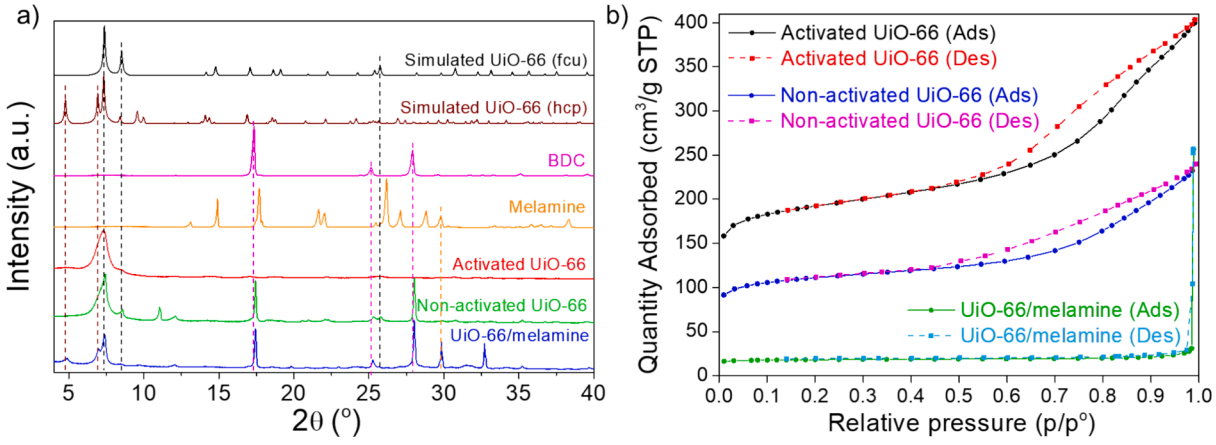

Fig. 4. a) XRD spectra of UiO-66 and UiO-66/melamine flame retardant samples. spectra of BDC, melamine and simulated UiO-66 (fcu and hcp phases) using Mercury 3.8 software [43] and CCDC 1018045 [44] for the fcu phase and CCDC 1854712 [49] for the hcp phase obtained from Cambridge Crystallographic Data Centre. b) Adsorption and desorption isotherms of different UiO-66 and UiO-66/melamine samples.

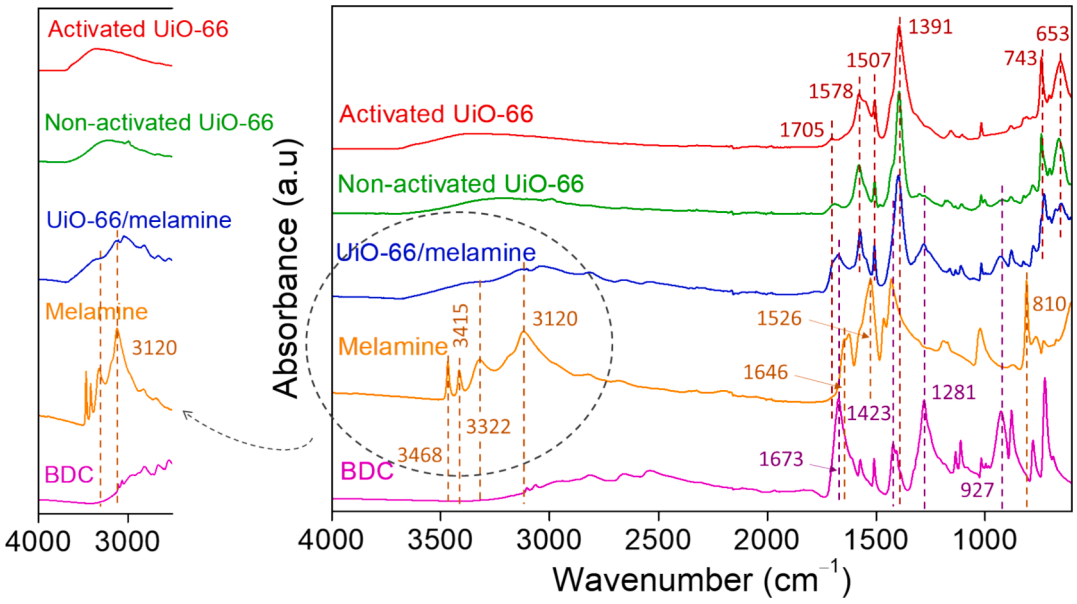

Fig. 5. FTIR spectra of different UiO-66, UiO-66/melamine, melamine and BDC samples.

addition, there is a peak at 1391 cm^{-1} that corresponds to the C-O bond present in the UiO-66 sample. In this sample, there are also peaks at 1507, 1578, 743 and 653 cm^{-1}, which are attributed to UiO-66 as mentioned above. These findings confirm the formation of UiO-66 and the presence of melamine and BDC in the UiO-66/melamine sample.

The thermal behaviour of the flame retardant samples was also evaluated using TGA, as shown in Fig. 6a. The derivative thermogram (DTG) curves are represented in Fig. 6b. For the activated UiO-66, there is a weight loss before 100 °C due to the absorbed water. Thermal stability is maintained until 500 °C, when the connecting bonds between the metal cluster and the ligand break, causing the structure to collapse. In the case of the non-activated UiO-66, there is an initial weight loss, likely due to the unreacted ligand and the structural template (TEABr), as this sample was only partially washed with ethanol. This loss corresponds to 30 wt% of sample weight up to 400 °C. Then, at 500 °C, the structural ligand degradation takes place and the lattice collapses. For the UiO-66/melamine sample, there is a slight decrease related to moisture. After that, there are two different weight losses: the first (9.6 wt%) from 200 to 270 °C is probably related to melamine and the second (32.7 wt%) from 270 to 350 °C, is caused by the BDC ligand. Since the thermal decomposition of melamine and BDC occurs at similar temperatures, part of the sample was washed abundantly with warm ethanol and dried at 100 °C. The TGA curve of this sample then only shows the second weight loss. XRD and FTIR analysis confirm the presence of residual BDC and the removal of melamine after the washing (see Figure S1, S2, and S3). Finally, at about 500 °C, the UiO-66 structure degrades. In this case, the percentage related to MOF formation is lower than for the UiO-66 samples, which is due to the low crystallinity of UiO-66 observed by XRD.

The particle morphology of the UiO-66 and UiO-66/melamine samples was observed under SEM, as shown in Fig. 7. The UiO-66 samples (both properly activated and non-activated) are uniform and present similar diameters (50.5 ± 7.3 nm and 60.4 ± 8.5 nm, respectively). Although they look slightly agglomerated, the particles can be measured accurately. The sample with melamine has a similar particle size (49.1 ± 9.4 nm), although the particles are not as homogeneous as those of the UiO-66 sample. This may be due to the presence of BDC and melamine crystals as observed by XRD (Fig. 4a).

For a clearer view of the UiO-66 structure, the samples were observed using TEM. The images obtained are shown in Figure S4. In the case of activated UiO-66 (Figure S4 a1, a2) the morphology is mainly spherical and presents agglomerated particles. For the non-activated UiO-66 sample (Figure S4 b1, b2), the appearance is less defined, showing diffuse particle edges probably due to the fact that this sample is less washed and there are residues of reagents around the solids. The particle morphologies in the UiO-66/melamine sample are less geometric. This is related to the presence of BDC and melamine around the UiO-66 nanoparticles (Figure S4 c1, c2). The particle sizes are slightly

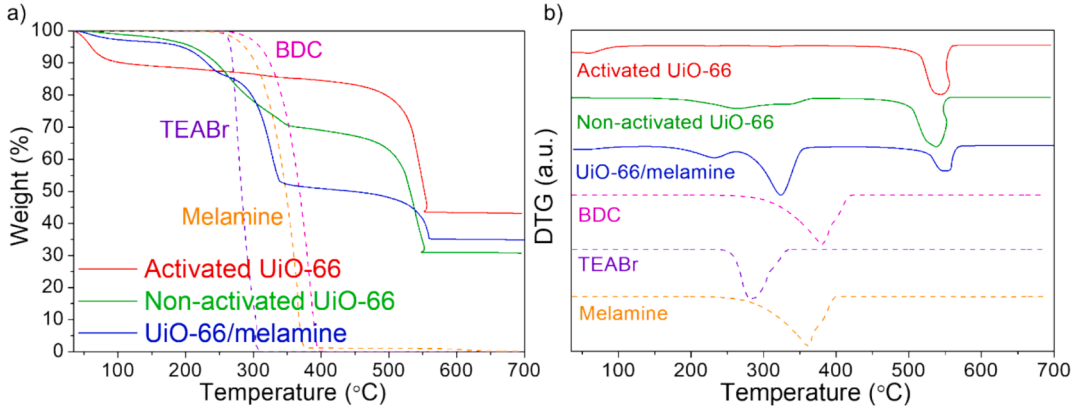

Fig. 6. a) TGA and b) DTG curves of UiO-66 (activated and non-activated) and UiO-66/melamine, BDC, TEABr and melamine.

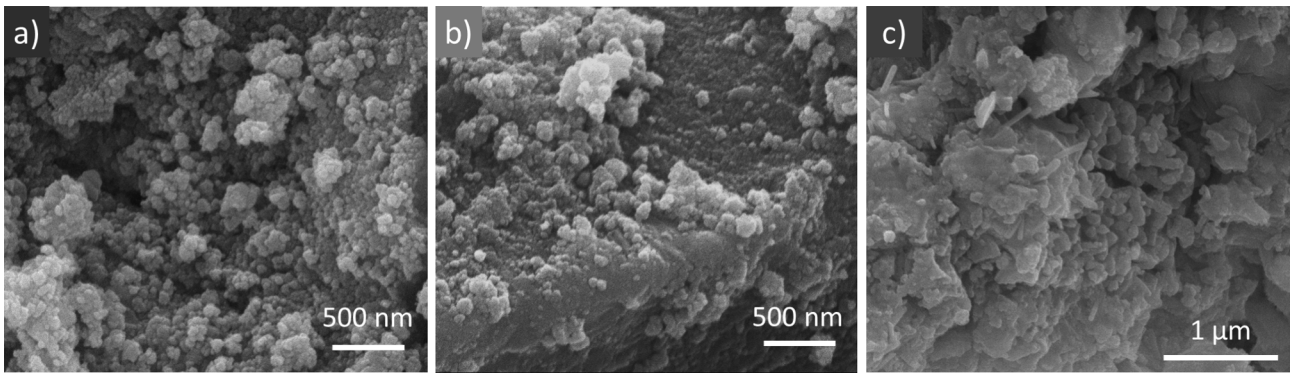

Fig. 7. SEM images: a) Activated UiO-66, b) Non-activated UiO-66 and c) UiO-66/melamine.

smaller than those observed by SEM, namely 37.5, 50.5 and 38.5 nm for activated UiO-66, non-activated UiO-66 and UiO-66/melamine, respectively.

Composites characterization

The PA6 composites were characterized using similar techniques to those used for flame retardant samples. Among the different percentages tested, the composites more characterised are those with a 4 wt% flame retardant load, which show a good fire performance results. In addition, lower percentages of flame retardant load, may not be detected by some of the characterization techniques.

The X-ray diffraction of the composites was measured to determine if the crystalline structure of the UiO-66 remained after the extrusion with polyamide. Fig. 8a shows the spectra obtained for PA6 and the composites after the incorporation of the flame retardant samples.

This figure shows that the crystalline peaks corresponding to UiO-66 with a fcu structure are in the spectra of the composites with activated and non-activated UiO-66. Particularly, the most intense peaks appear at 7.4° and 8.5°. In the same way, the XRD spectrum of the UiO-66/melamine composite shows peaks at 4.7°, 7° and 7.3° corresponding to the hcp structure of UiO-66. Therefore, the presence of UiO-66 within the polymeric composites is confirmed. In the spectrum of pure PA6, the characteristic peaks related to the crystallographic α-phase of polyamide are visible at 20.7° and 23.2° [34]. The composites with the flame retardant materials also show these typical peaks of the polyamide, indicating that the incorporation of the UiO-66 does not affect the polymer conformation. In addition, the crystallinity is higher for the composite sample with UiO-66/melamine, as indicated by these peaks. This property is further calculated by DSC analysis of the composites.

The FTIR spectra of PA6 composites with 4 % or 7 % loads are shown in Fig. 8b, where the low amount of flame retardant makes detection more challenging. Nevertheless, some bands assigned to UiO-66 appear in the PA6 composites but not in the pure PA6 sample. In the highlighted region around 3500 cm^{-1}, there is a shoulder related to the UiO-66 and UiO-66/melamine samples. This strong and broad absorption band may be attributed to the presence of hydrogen-bonded water molecules physisorbed on the surface or within the crystalline water [59]. In addition, the small peak at 1705 cm^{-1} corresponding to C=O stretching in non-dissociated acid groups of UiO-66 is present in the PA6 composites. Finally, in the low wavenumber region, two peaks appear at 1018 cm^{-1} and 880 cm^{-1}, corresponding to peaks present in the flame retardant spectra and absent in the pure PA6 polymer.

The thermal stability of the composites has been tested using TGA equipment under air atmosphere. Fig. 9 shows the TGA and DTG curves of flame retardant solid samples (discontinuous lines) and of the composites (continuous lines) with and without the particles.

In the pure PA6 polymer curve, the large mass loss is related to the degradation of the polyamide at around 350 °C, with a maximum value in DTG at 447 °C. In the composites with flame retardant samples, the polymer degradation occurs earlier than in the case of pure PA6. This faster degradation might be due to a slight catalytic effect of the UiO-66 incorporated during the composites' preparation. The maximum peaks of weight loss obtained from the DTG of PA6 composites with UiO-66, non-activated UiO-66 and UiO-66/melamine are 423 °C, 422 °C and 439 °C, respectively. This earlier degradation of PA6 is more noticeable in the UiO-66 samples than in the UiO-66/melamine ones, which have a lower proportion of UiO-66 compared to the pure UiO-66 sample. In the DTG curve (Fig. 9b) of PA6/4% UiO-66/melamine, there is a detectable weight loss before the polymer degradation, around 300 °C, which could

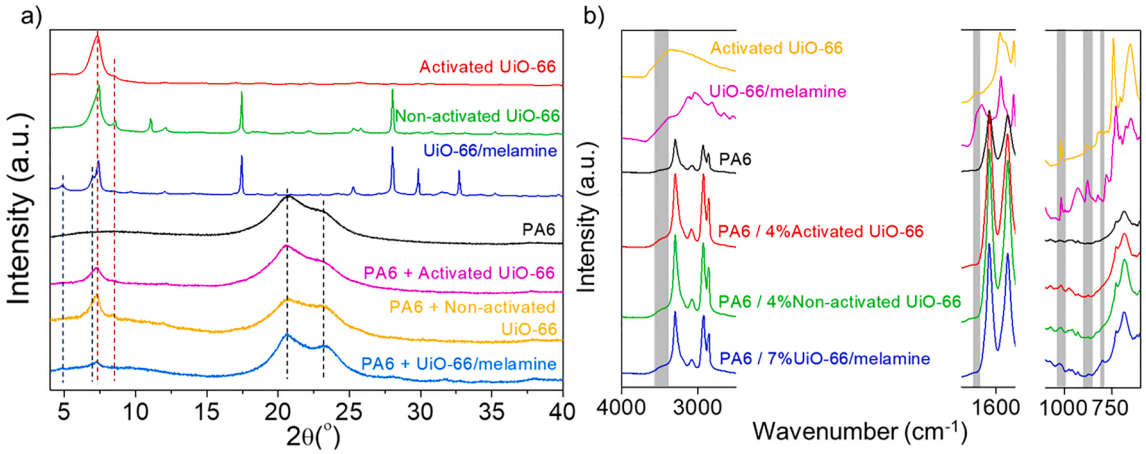

Fig. 8. a) XRD and b) FTIR spectra of flame retardant samples, and PA6 composites (4 wt% of flame retardants unless indicated) and PA6.

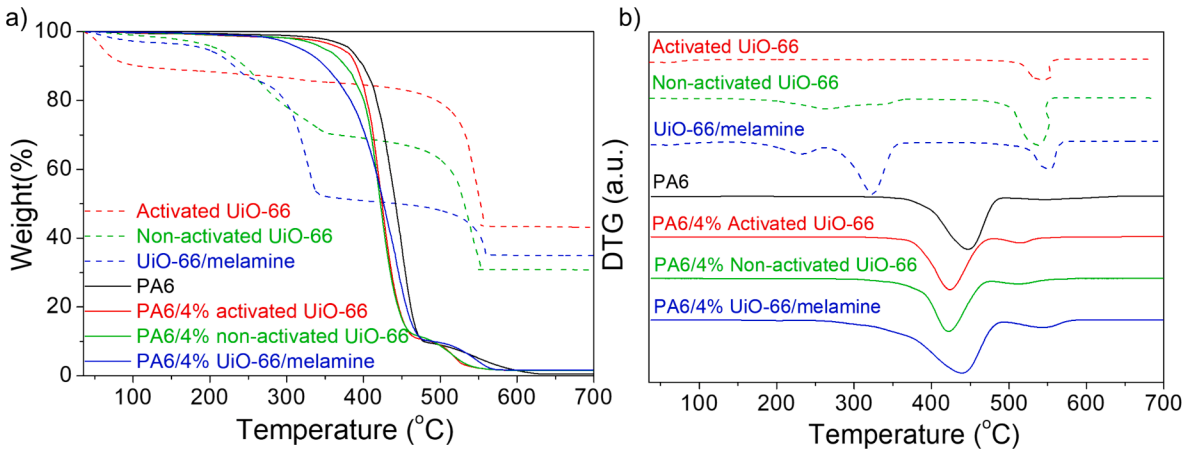

Fig. 9. a) TGA and b) DTG curves of flame retardant samples, PA6 composites (PA6/4% activated UiO-66, PA6/4% non-activated UiO-66, PA6/4%UiO-66/melamine) and PA6.

correspond to the melamine and BDC. In addition, in the polymer composites with flame retardant, a small weight loss is observed after the degradation of the polymer (~475 °C), which may be due to the presence of the MOF. However, the pure PA6 also shows a weight loss, although it is less abrupt than that observed for the composites with MOF. The caloric effects produced by the degradation of the polymer may cause this acceleration in the degradation of the MOF.

It should be noted that the final residue of the TGA carried out under air atmosphere is zirconium oxide (ZrO_2), and it is possible to determine its amount in the samples after each analysis. Consequently, the amount of UiO-66 in the composite can be calculated, considering that 6 mol of Zr are required to form 1 mol of UiO-66 ($Zr_6O_4(OH)_4(BDC)_6$). The final percentages remaining for PA6 composites were 1.55 wt%, 1.56 wt% and 1.23 wt% for activated UiO-66, non-activated UiO-66 and UiO-66/melamine, respectively. Table 2 shows the experimental values calculated by TGA, which are quite close to the theoretical values.

For non-activated UiO-66, the weight percentage corresponding to the moisture and ligand (~30 wt%) has been subtracted from the total weight loss when calculating the experimental percentage of flame retardant added to the polymers. Similarly, for the UiO-66/melamine sample, the weight losses related to BDC (32.7 wt%) and melamine (9.6 wt%) observed in the TGA curve have been taken into account.

Additionally, the thermal properties of the composites are characterized by DSC. This analysis is used to determine, crystallization and melting temperatures, and their enthalpies are calculated by integrating the peaks. Furthermore, the degree of crystallinity is calculated using equation (1). These values are presented in Table 3.

According to the data obtained from the calculation of the crystallinity degree, it can be observed that increasing the additive also increases crystallinity. This could potentially enhance flame retardant behaviour, as combustion is more difficult in crystalline materials than in more amorphous ones.

Fig. 10 shows the DSC curves of composite samples during the cooling period and the second heating. The crystallization temperatures (T_c) for each composite can be observed in Fig. 10a. Materials containing flame retardant exhibit a T_c around 189–187 °C, slightly lower than that of pure PA6 (192 °C). Fig. 10b represents the second heating curves. It is noticeable that the pure PA6 sample displays a shoulder around 213 °C in addition to the main peak at 220 °C. The shoulder and peak describe two crystalline forms of PA6: γ, which melts earlier, and α, the most thermodynamically stable [60]. Hence, the presence of UiO-66 and melamine appears to promote the transition to the α crystalline form of PA6. However, this transition is not clearly observed in the XRD analysis (Fig. 8a).

XPS was used to characterise the PA6 composites and to determine how their atomic compositions varied with the incorporation of flame retardants. Fig. 11 shows the high resolution Zr 3d spectra for the PA6 samples obtained with the incorporation of activated UiO-66 (Fig. 11b) and UiO-66/melamine (Fig. 11d). As can be observed in all samples the Zr 3d spectra present the two typical diffraction peaks of zirconium at ~182.6 eV and 185 eV, corresponding to Zr 3d5/2 and Zr 3d3/2, respectively [27]. Therefore, the presence of UiO-66 in the PA6 composites can be proved. Fig. 11a shows the main peaks of PA6 attributed to C–C/C=C at 285 eV, C-N at 286 eV, C=O (including N-C=O bonds) at 287.97 eV, and O-C = O at 288.75 eV. For the PA6 composites with activated UiO-66 (Fig. 11c) the contribution of the C-O and C=O bonds increases in comparison to pure PA6 due to the presence of carbonyl groups of UiO-66. In the case of PA6 composites with the UiO-66/melamine sample (Fig. 11e), the components in the C region show more changes. The presence of melamine and UiO-66 is indicated by the increase in the C-O/C-N (285.96 eV) and C=O (287.98 eV) peaks.

The atomic percentages and their corresponding C/O, C/N and C/Zr ratios for all samples are shown in Table 4. This table also confirms the presence of zirconium in the PA6 composites. The PA6 composite with the UiO-66/melamine sample shows a significant increase in the nitrogen percentage, which is attributed to the presence of melamine. As a result, the C/N ratio considerably decreases in comparison to the pure PA6 composite. Its values are 19.4 and 6.5 for PA6 and PA6 + UiO-66/melamine, respectively.

Table 2
Experimental percentage of flame retardant inside the PA6 composites. The theoretical value is 4 wt%.

Polymer	Sample	wt% flame retardant
PA6	Activated UiO-66	3.50
	Non-activated UiO-66	5.02
	UiO-66/melamine	4.79

Table 3
DSC results; T_c: crystallization temperature; ΔH_c: crystallization enthalpy; T_m; melting temperature; ΔH_m: melting enthalpy; X_c: crystallization degree.

Sample	T_c (°C)	ΔH_c (J/g)	T_m (°C)	ΔH_m (J/g)	X_c (%)
PA6	192	−64.9	213/220	59.2	31.0
PA6 + Activated UiO-66	189	−64.5	220	57.2	31.2
PA6 + Non-activated UiO-66	189	−64.2	221	64.7	35.3
PA6 + UiO-66/melamine	187	−79.3	218	69.0	37.6

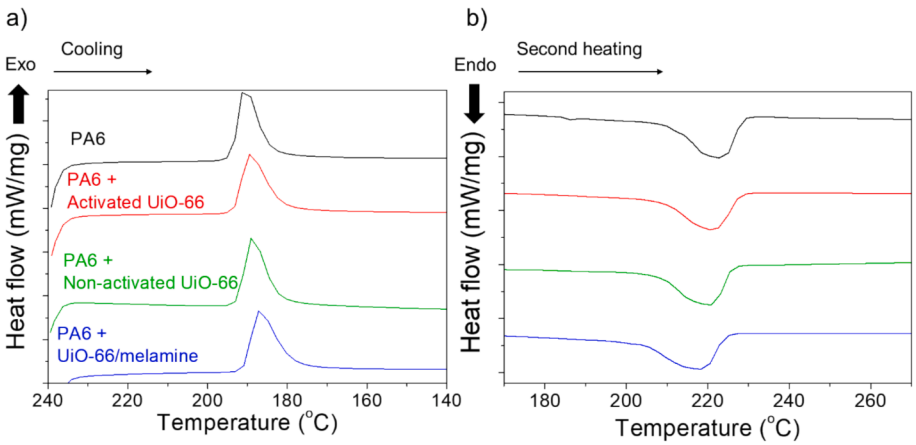

Fig. 10. DSC curves of PA6 and composites with 4 wt% of flame retardants: a) Crystallization temperatures, b) Melting temperatures.

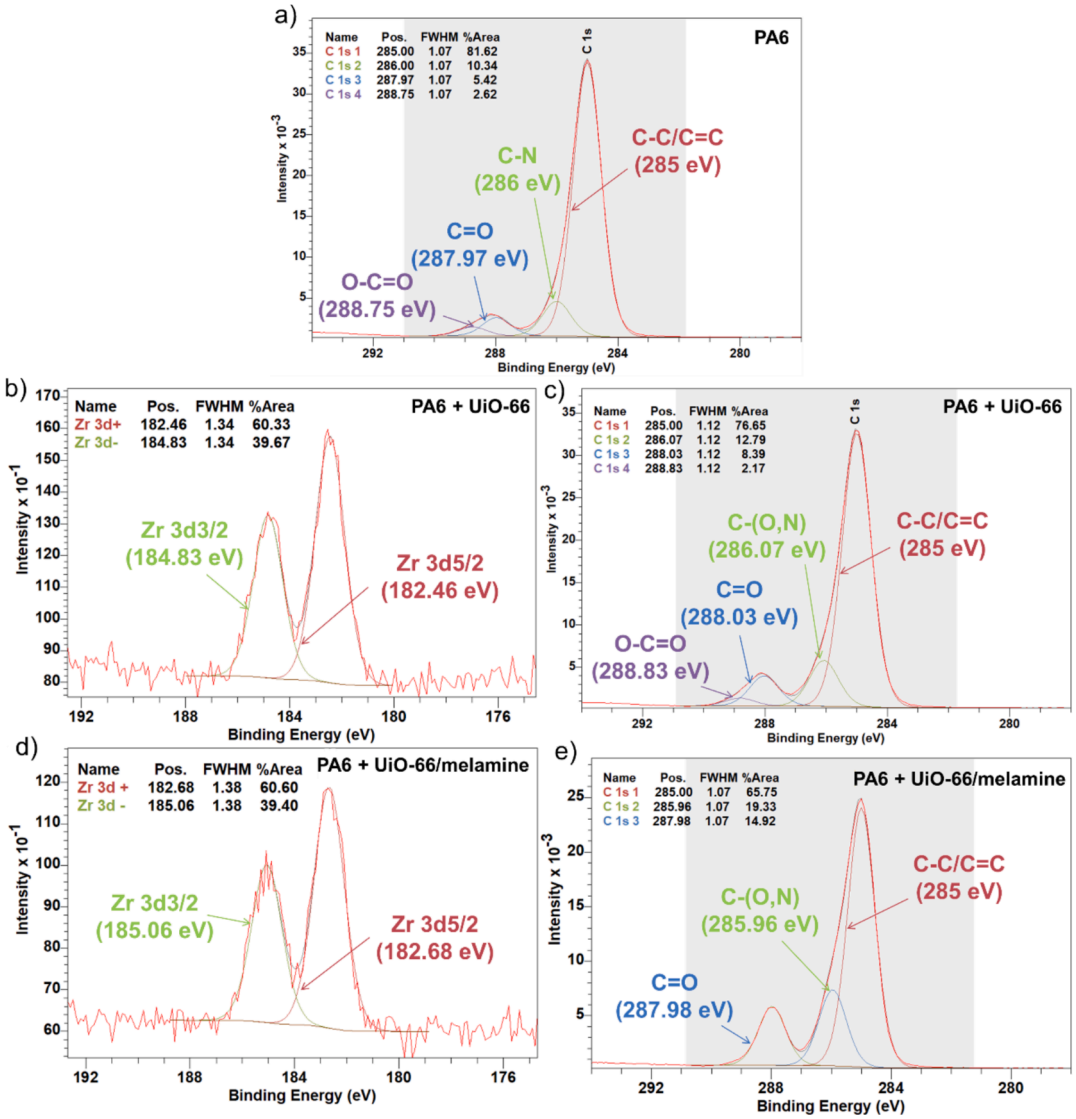

Fig. 11. XPS high resolution of composites: a), c) and e) C 1 s spectra of pure PA6, PA6 + 7 wt% activated UiO-66, and PA6 + 7 wt% UiO-66/melamine, respectively; b) and d) Zr 3d spectra of PA6 + 7 wt% activated UiO-66, and PA6 + 7 wt% UiO-66/melamine, respectively.

Table 4
Atomic percentages and C/O, C/N and C/Zr ratios of PA6 composites obtained by XPS analysis. The burned samples measured correspond to the point 2 marked in Fig. 17.

		at.% C	at.% O	at.% N	at.% Zr	C/O	C/N	C/Zr
PA6	**Initial**	83.90	11.78	4.32	–	7.1	19.4	–
	Burned	85.77	12.94	1.29	–	6.6	66.5	–
PA6 +	**Initial**	79.99	13.99	5.90	0.12	5.7	13.5	667
activated UiO-66	**Burned**	81.72	14.11	4.17	0.10	5.8	19.6	817
PA6 + UiO-66/melamine	**Initial**	75.69	12.65	11.55	0.11	6.0	6.5	688
	Burned	75.94	12.58	11.37	0.11	6.0	6.7	690

The presence and the correct distribution of the flame retardants inside the composites are confirmed using SEM. Moreover, EDX analysis is employed to verify the presence of UiO-66 and analyse the chemical composition of the composite materials. Fig. 12 shows cross-sectional images of PA6 composites. In Fig. 12 a, the pure PA6 polymer is depicted with no observable particles. In contrast, in the composites containing flame retardant samples (Fig. 12 b, c, d), UiO-66 particles are visible, although some regions exhibit a slight agglomeration. The EDX analysis conducted in these areas confirms the presence of zirconium in the particles observed on the cross-sectional surfaces. A mapping analysis was also performed on these samples and the green dots show to the presence of zirconium. Therefore, this analysis also confirms the effective integration of the flame retardant samples within the composites.

PA6 composites were prepared with a load of 7 wt% of activated UiO-66 and UiO-66/melamine. In the sample containing only UiO-66, the particles were not evenly distributed within the specimen, as evidenced by large agglomerations on the surface. Fig. 13a, shows a particle agglomeration larger than 100 μm. Therefore, the load increase hinders good particle dispersion. Conversely, in the sample with melamine, the particles are uniformly dispersed throughout the composite (Fig. 13b) with no significant particle agglomerations. This improved dispersion may be attributed to the presence of free BDC and melamine, which potentially act as compatibilizers during polymer processing.

The mechanical properties of the composites after the incorporation of flame retardants were also analysed to ensure a good performance of these materials. Table 5 summarises the results obtained from different mechanical tests.

Firstly, the incorporation of flame retardants slightly increases the tensile modulus (from 3361.1 to 3538.4 and 3441.7 MPa for PA6, PA6 + activated UiO-66 and PA6 + UiO-66/melamine, respectively). The reported values for PA6 are in a range of 2800–3400 MPa [61,62] and can be increased by incorporating flame retardants [2]. This parameter measures the stiffness of a material, and its increase with the addition of flame retardants is therefore due to the greater force required to deform it at the expense of ductility. The tensile strength and % elongation at yield indicate the material's ability to withstand loads and forces during its lifetime. This value decreases with the addition of flame retardants, due to reduced flexibility and limited ability to orientate in PA6 chains [2]. The brittle behaviour shown for PA6 with flame retardants is indicated by the decrease of elongation at break, which could be due to cracks caused by the incorporation of solids. Moreover, the higher crystallinity degree of PA6 + UiO-66 (or UiO-66/melamine) (see Table 3 from DSC results) is also related to the decrease in flexibility and ductility.

The Charpy impact strength test indicates how much energy a material can absorb before fracturing. It is therefore a way of determining how brittle or ductile a material is. As observed, the incorporation of flame retardants results in a brittle material, so the Charpy impact is reduced. The HDT value is slightly reduced by 2 °C, so it can be said that the incorporation of flame retardant has no effect on this parameter.

Fire retardant performance

The melt dripping and UL-94 classification results for PA6 composites are summarized in Table 6. Pure PA6 receives an NR classification, indicating that at least one of the five specimens tested burned for more than 30 s and the flame did not extinguish. The materials with a significant load of flame retardants exhibit an improved fire behaviour. The results obtained for each additive depend on the type of polyamide used in each case. Therefore, each composite is compared with the same kind of PA6 used in its preparation. The extinguishing times are calculated as the average of five samples for each flame application. The data obtained for the UL-94 test are presented in Table 6. For the estimation of the extinguishing times (t_1 and t_2), when the flame did not self-extinguish after 30 s (time from which the classification is established as NR), 30 s is the value considered to obtain the average extinguishing time. Moreover, Fig. 14 illustrates the accumulated time intervals required for flame extinction.

As shown, PA6 materials with activated UiO-66 gradually reduce the extinction time with increasing additive load (1 %, 2 % and 4 %), showing the best result with a 4 % load and achieving a V-2 classification. In the case of non-activated UiO-66, samples with a load of 1 % and 2 % do not show any improvement in burning time. A 4 % load is necessary to detect a decrease in extinction time. When comparing both samples, the activated UiO-66 offers better results at low loads. However, with a 4 % of load, both samples provide similar results in terms of extinction time and dripping behaviour. This can be due to the fact that the non-activated UiO-66 sample contains less MOF than the activated UiO-66 one. Therefore, a larger amount of non-activated sample is necessary to produce a fire retardant effect.

As explained in the literature [26], the key factor influencing flame retardancy with the incorporation of MOF is the formation of char on the composite surface. In the case of UiO-66, zirconia is generated from the pyrolysis and oxidation, and is able to catalyse the conversion of soot and CO into char residue [29]. Moreover, zirconia is a high-temperature refractory material that is generally used in the fabrication of thermal barrier coatings [63], which reduces the diffusion rate of volatile compounds and the oxygen supply to the interior of the sample. Therefore, this compound acts as an insulating material, slowing down heat transfer and restraining the spread of pyrolysis products from the PA6 composite to the burning zone [27]. In addition, UiO-66 can adsorb gases and smoke before its degradation occurs.

The UiO-66/melamine sample exhibits an excellent fire retardant performance. The sample with 1 % of UiO-66/melamine has shorter extinguishing times than composites with the same percentage of only UiO-66. When the additive load is increased to 2 % and 4 %, the composites achieve a UL-94 classification of V-2. Among these, the 4 % UiO-66/melamine sample has the shortest extinguishing time. This sample also shows the best dripping behaviour, since only one out of five tested samples burns the cotton during the first ignition. Although, four out of five samples burn it during the second ignition, the flame does not reach the specimen. Notably, one out of five tested samples achieves the best classification in the UL-94 test, V-0. However, in the case of the samples that do not contain melamine, all five tested samples burn the cotton in each flame application. The flame retardant effect of melamine lies in its ability to absorb significant amounts of heat during its endothermic sublimation, release inert ammonia, which dilutes oxygen and combustible gases in the gaseous phase, and form a thermally stable residue [64].

When the load is increased to 7 wt%, the UiO-66 sample does not

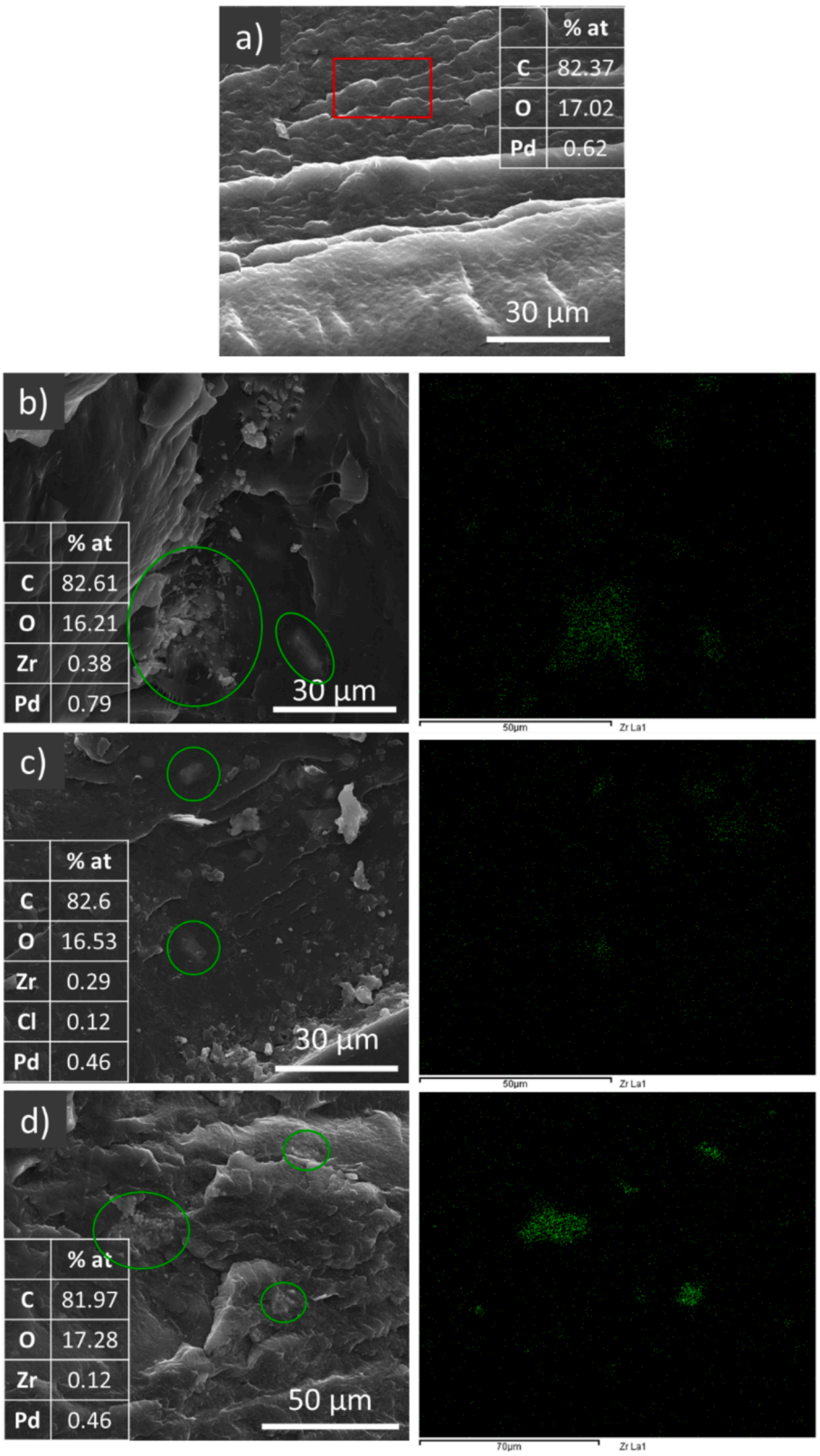

Fig. 12. SEM cross-section images of PA6 composites with 4 wt% of flame retardant and their corresponding mapping for Zr (green): a) Pure PA6 b) PA6 + activated UiO-66, c) PA6 + non-activated UiO-66, d) PA6 + UiO-66/melamine.

show a good fire retardant performance. The flame extinguishing times are similar to those of the pure PA6 composite. In both cases, the samples do not meet the conditions of UL-94 test and cannot be classified according to this standard. The reason for this worse behaviour with the increased load could be related to the particle agglomeration (see Fig. 13). However, in the case of the UiO-66/melamine sample, the times after each flame application are slightly shorter than those obtained with a load of 4 wt%, while the dripping behaviour does not

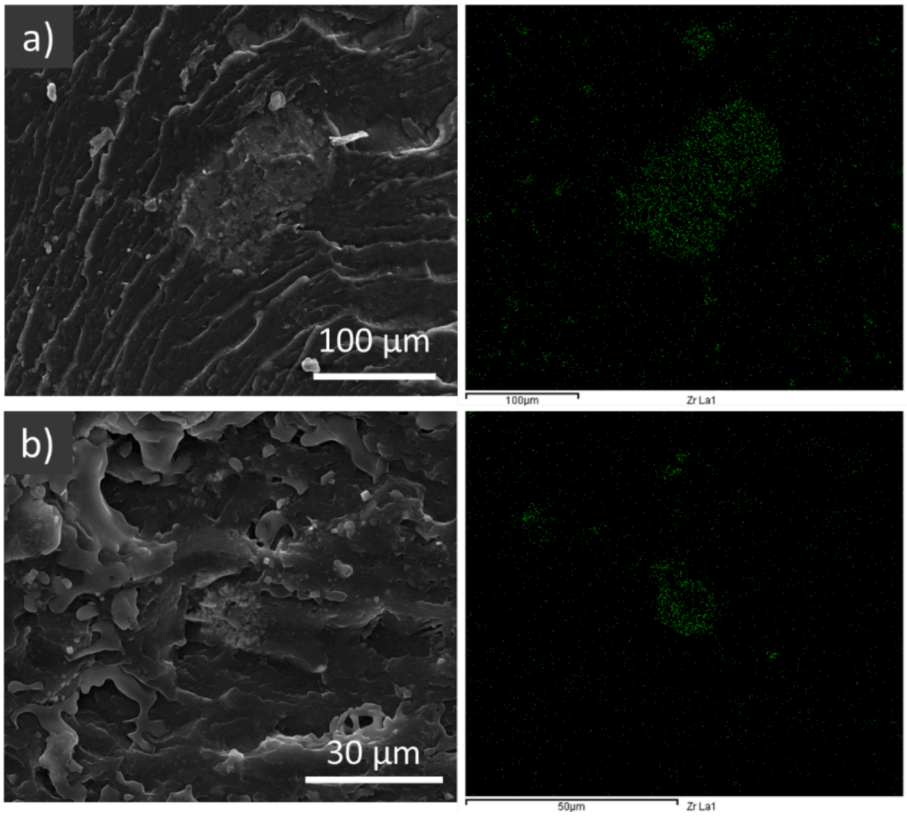

Fig. 13. SEM images of PA6 composites with 7 wt% of flame retardant and their corresponding mapping for Zr (green): a) Activated UiO-66 and b) UiO-66/melamine.

Table 5
Mechanical properties of PA6 composites.

Mechanical properties	Units	PA6	PA6 + 7 % activated UiO-66	PA6 + 7 % UiO-66/ melamine
Tensile modulus	MPa	3361.1 ± 47.0	3538.4 ± 40.2	3441.7 ± 100.3
Tensile strength at yield	MPa	85.33 ± 0.14	46.25 ± 2.49	43.57 ± 0.21
Elongation at yield	%	3.823 ± 0.024	1.399 ± 0.096	1.303 ± 0.002
Tensile strength at break	MPa	53.82 ± 3.07	41.18 ± 7.96	38.76 ± 10.01
Elongation at break	%	11.272 ± 0.625	1.484 ± 0.257	1.320 ± 0.272
Charpy notched impact strength	kJ/ m^2	2.813 ± 0.936	1.336 ± 0.086	1.508 ± 0.600
Heat Deflection Temperature (HDT)	°C	58.5	56.5	57.9

improve compared to the 4 wt% sample. Therefore, the classification in the UL-94 test remains V-2.

In addition, the horizontal burning test was performed on the PA6 composites with a load of 7 wt%. This test determines the linear combustion rate at which the specimens are burned. Fig. 15a shows a photo of the samples obtained after this analysis. It can be seen that the pure PA6 composites are more consumed by the fire than the samples that contain the flame retardants, since in two specimens the fire exceeded the first mark. However, in the PA6 samples with activated UiO-66 the flame was extinguished earlier, and the fire did not reach the first mark in any of the specimens. In the case of the PA6 with UiO-66/melamine sample, the improvement is more notable. The length of the specimen consumed by fire was very short, it remained practically whole after the test.

As previously explained, the linear combustion rate was calculated between the two marks in the sample, and since the fire did not reach the second mark in any of the samples, the combustion rate value could not be calculated. Therefore, according to the standard rule, this value is zero. In any case, the fire retardant effect is visually shown in the photos (Fig. 15a).

The LOI test results are represented in Fig. 15b. Compared with PA6, the LOI values of PA6 + activated UiO-66 and PA6 + UiO-66/melamine, both composites with a load of 7 wt%, were improved from 22.4 % to 23.2 % and 35.5 %, respectively. The outstanding result achieved in this test aligns with the results of the vertical and horizontal burning tests, where the UiO-66/melamine sample demonstrated excellent flame retardant properties.

Fig. 16 shows a schematic representation of the flame retardant mechanism that takes place during the combustion of polyamide with and without the incorporation of flame retardant materials, as explained for UiO-66 and melamine.

The burned specimens with flame retardant materials are also characterized by XRD, SEM-EDX and FTIR applied to different points of the samples to determine how the chemical composition varies along the burned sample. The efficacy of the flame retardant is evidenced by the visual appearance of the samples, with PA6 being more consumed by fire than the specimens with incorporated of flame retardants, especially the sample with melamine, which is the least affected (Fig. 17a). In the samples with activated UiO-66, the analyses confirm an increase in the atomic percentage of zirconium (see Fig. 17b) due to the formation of zirconium oxide after combustion, along the length of the specimen, with the highest zirconium percentage at the most burned edge of the sample (point 1). Looking at the XRD spectra of the polymeric samples with activated UiO-66 (Fig. 17b), after the combustion, the peaks related to UiO-66 are more intense at the burned edge (point 1) while those corresponding to PA6 decrease. In the UiO-66/melamine samples, the

Table 6
UL-94 test results and dripping behaviour for different flame retardant (FR) percentages. Five different samples are measured for each material.

Sample	% FR	UL-94 test			Dripping	
		Classification	t_1 (s)[1]	t_2 (s)[1]	First ignition[2]	Second ignition[2]
PA6 (1)	–	NR	12.8 ± 7.9	15.4 ± 13.8	5/0	5/2
PA6 (1) + Activated UiO-66	**1 %**	NR	21.8 ± 11.2	23.0 ± 9.6	5/2	5/3
	2 %	NR	12.7 ± 10.7	15.1 ± 10.6	5/0	5/1
	4 %	V2	5.4 ± 0.7	10.4 ± 8.6	5/0	5/0
PA6 (1) + Non-activated UiO-66	**1 %**	NR	15.1 ± 13.7	19.0 ± 10.3	5/2	5/2
	2 %	NR	16.0 ± 13.2	17.7 ± 13.2	5/2	5/2
	4 %	V2	9.8 ± 11.4	4.7 ± 2.0	5/0	5/0
PA6 (2)	–	NR	18.0 ± 9.5	22.5 ± 11.1	5/0	5/0
PA6 (2) + UiO-66/melamine	**1 %**	NR	3.2 ± 1.9	12.7 ± 10.9	5/0	5/0
	2 %	V2	3.1 ± 1.0	4.5 ± 3.1	4/0	3/0
	4 %	V2 (V0 in one sample)	2.3 ± 0.3	2.7 ± 2.3	1/0	4/0
PA6 (3)	–	NR	18.7 ± 13.9	21.3 ± 12.2	5/0	5/0
PA6 (3) + Activated UiO-66	**7 %**	NR	19.7 ± 9.6	11.1 ± 12.1	5/0	5/0
PA6 (3) + UiO-66/melamine	**7 %**	V2	2.2 ± 0.6	1.9 ± 0.3	1/0	4/0

[1] Average value and deviation of the five samples tested.
[2] Number of samples that set cotton on fire / number of samples in which the flame reaches the support.

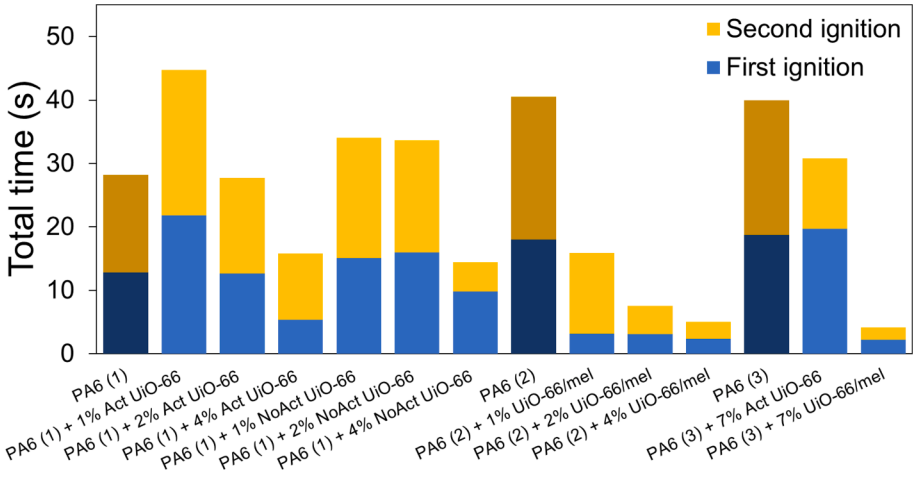

Fig. 14. Total period of time necessary to extinguish the flame after two applications in the UL-94 vertical test.

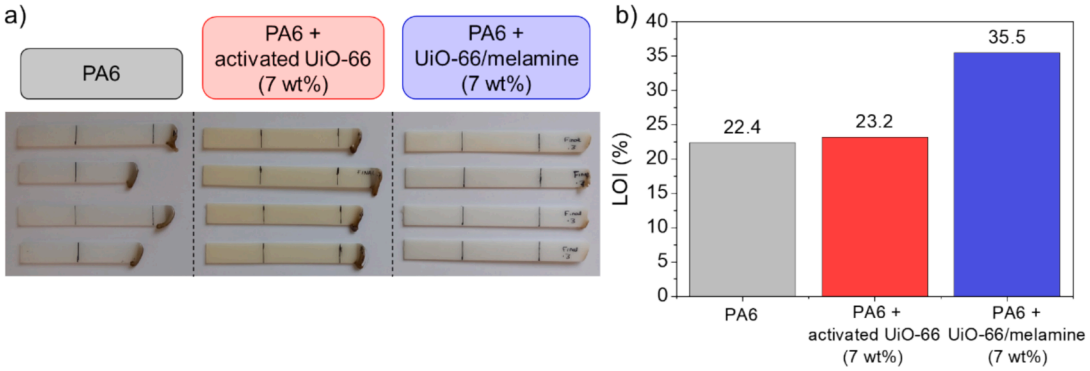

Fig. 15. a) PA6 composites obtained after horizontal burning test with and without flame retardant samples. four specimens are analysed for each case. b) LOI results of PA6, PA6 + activated UiO-66 and UiO-66/melamine.

changes in the EDX and XRD analyses (Fig. 17c) are barely noticeable and, the composite maintains its composition and structure, which is in accordance with the photographs of the burned samples and the results of the flammability tests. A FTIR analysis (Fig. 17d, e) was also performed to confirm the observed changes, however as with the polymeric composites before combustion, the spectrum of PA6 is predominant in the analysis, and no other peaks are visible (Fig. 17d, e).

XPS was used to characterise the PA6 composites after the burning test performed in the fire retardancy evaluation. There is no significant difference in the binding energy for Zr 3d spectra (see Fig. 11 and, Fig. S5), since the oxidation state in ZrO_2 has a binding energy (182.4 eV) similar to that of the UiO-66 [65]. The burned sample of PA6 maintains the same peaks of the C 1s spectra although the percentage of each varies, with a decrease in those related to C-N and C=O bonds (Figure S5). For the PA6 composites with activated UiO-66 and UiO-66/melamine (Fig. 11c, e), the same peaks appear after the burning test, but

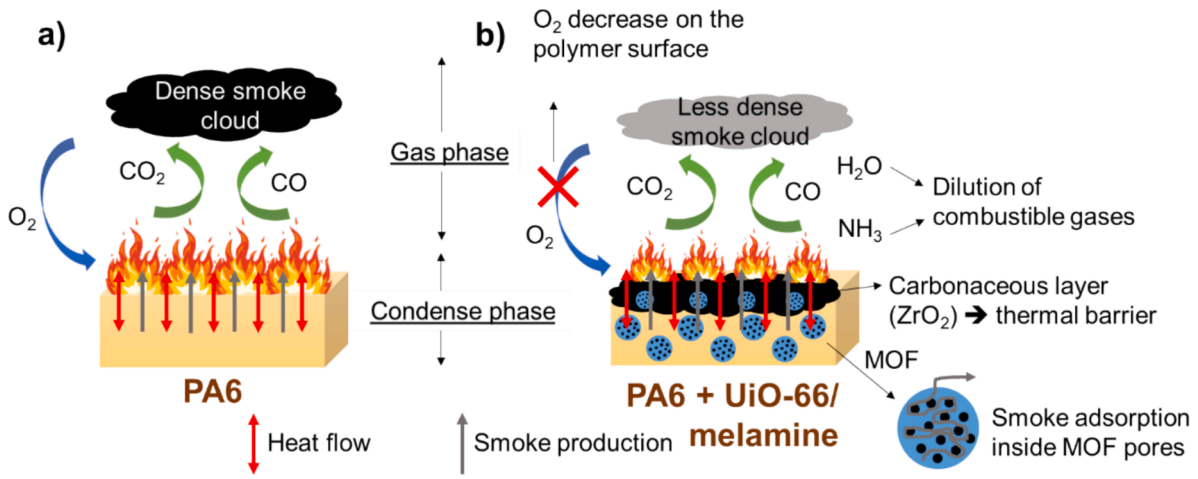

Fig. 16. The flame retardant mechanism that happens during the combustion of a polyamide sample with and without the addition of the flame retardants.

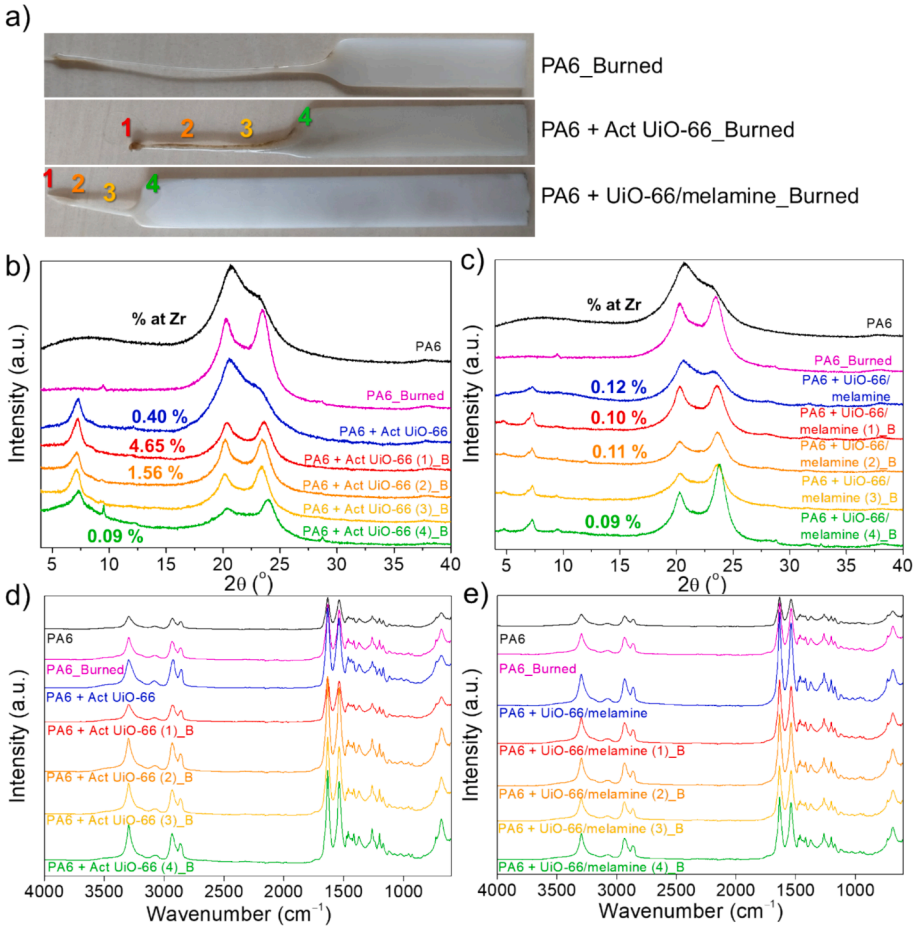

Fig. 17. Characterization of burned specimens after the UL-94 burning test: a) Photograph indicating positions of analysis. b, c) XRD with Zr atomic percentage analysed by EDX for PA6 + 7 wt% of activated UiO-66 (b) and PA6 + 7 wt% of UiO-66/melamine (c). d, e) FTIR for PA6 + 7 wt% of activated UiO-66 (d) and PA6 + 7 wt% of UiO-66/melamine (e).

their intensity is slightly modified. The atomic percentages of C/O, C/N and C/Zr ratios (Table 4) are very similar before and after the burning test.

Table 7 shows a comparison of the results obtained in the UL-94 test and LOI for different polymers in the literature, detailing the type of polymer used and the load. As observed in the table, the required loads used in other studies to achieve a V-0 rating are higher than those used in this work. It is known that melamine has good fire retardant properties when incorporated into polymers, such as polyamide 6, polypropylene (PP), or low-density polyethylene (LDPE) [66], reducing burning time and improving flame retardancy, achieving a V-0 classification and LOI values of 24.1 and 25.9 % with a load of 10 or 20 wt%, respectively. Furthermore, melamine in combination with organic clays has shown an excellent fire retardant performance (V-0 in UL-94 test and

Table 7
Comparative table results obtained in the UL-94 test.

Type of polymer	Flame retardant	% Load (wt%)	UL-94	LOI (%)	Ref.
PA6	–	–	Burning	21.9	[66]
	Melamine	10	V-0	24.1	
		20	V-0	25.9	
PA6	–	–	V-2	21.0	[67]
	Melamine pyrophosphate (MPP)	25	V-2	29.5	
	Melamine-modified montmorillonite (MA-MMT) / MPP	2 / 23	V-0	32.0	
PA6	–	–	Burning	–	[68]
	Organophilic montmorillonite (OMT)	5	Burning	–	
	Decabromodiphenyl oxide (DO) / Antimony oxide (AO)	15 / 5	V-0	–	
	Melamine cyanurate (MCA)	15	V-0	–	
PA66	–	–	V-2	–	[69]
	Melamine	15	V-0	–	
PA66	–	–	V-2	–	[70]
	Melamine-modified layered silicate (MLS)	5	V-2	–	
	MLS / MCA	3 / 4	V-0	–	
PLA	–	–	Burning	18.1	[29]
	UiO-66-NH_2@TEP_{50}	2	V-0	26.4	
HIPS	–	–	Burning	18.8	[71]
	MCA + Aluminium hypophosphite + nano-SiO_2	3.7 + 14.8 + 1.5 %	V-0	26.9	
Epoxy	–	–	Burning	25.6	[31]
	UiO-66 – Prussian blue analogues (PDA) – polydopamine (PBA)	3	V-1	28.2	
PA6	–	–	V-2	23.0	[72]
	PEG/DDP	8	V-0	35.0	
PA66	–	–	V-2	24.0	[73]
	PPO/RP	14	V-0	41.0	
PA6	–	–	Burning	22.4	Our work
	UiO-66 and melamine	4	V-2	–	
	UiO-66 and melamine	7	V-2	35.5	

LOI value of 32 %) for polyamide 6 with the incorporation of 25 wt% of flame retardant samples [67]. Additionally, the flame retardancy of PA6 has been improved by incorporating organophilic clay (5 wt%) and conventional fire retardants, such as melamine cyanurate (MCA) (15 wt %) as well as the combination of decabromodiphenyl oxide (DB) (15 wt %) and antimony oxide (AO) (5 wt%). V-0 classification has been obtained with MCA and the mixture of DB/AO [68]. Studies in the literature show that the addition of 15 wt% of melamine into polyamide 66 (PA66) can achieve a V-0 rating with a non-flammable dripping mechanism [69]. In addition, melamine-modified layered silicate and/or MCA are incorporated into PA66, achieving an optimal result of V-0 with the combination of the two flame retardant samples [70]. For polymers other than polyamide, the flame retardancy is also tested. The addition of phosphorous flame retardant encapsulated within UiO-66-NH_2 has improved the flame retardant properties of polylactic acid (PLA), achieving a V-0 classification and LOI value of 26.4 % with a load of only 2 wt% [29]. Sun et al. studied the flame retardancy of high impact polystyrene (HIPS) using a 20 wt% load of a mixture of MCA/aluminium hypophosphite/nano-SiO_2, and obtained a V-0 classification and LOI value of 26.9 % [71]. To provide an epoxy (EP) with flame retardant properties, a hierarchical hybrid between UiO-66, Prussian blue analogue (PBA) and polydopamine (PDA) has been added to its composition. It has obtained a V-1 classification in the UL-94 V test and LOI value of 28.2 % [31]. A novel inherently flame-retardant thermoplastic polyamide elastomer was synthesised by Lu et al. [72], with phosphorus-containing groups (DDP), achieving a UL-94 V-0 rating and LOI value of 35 %. The flame retardancy of PA66/polyphenylene oxide (PPO) composites with the addition of $Al(OH)_3$-coated red phosphorus (RP) were studied and obtained a V-0 classification and LOI value of 41 % by incorporating 14 % of the flame retardants [73]. Therefore, the materials prepared in this work require a lower amount of flame retardant to achieve a great flame retardant behaviour.

Conclusions

UiO-66 with face centred cubic (fcu) crystal structure has been prepared by solvent-free synthesis using TEABr as a template. Replacing TEABr with melamine in the synthesis facilitates the formation of UiO-66, but as evidenced by XRD, the incorporation of melamine promotes the formation of another crystalline phase of UiO-66 (hexagonal closed packed, hcp). This sample, as confirmed by XRD, TGA and FTIR, is made up of UiO-66, melamine, and unreacted BDC.

The flame retardant behaviour of polymer composites incorporating UiO-66 improves when the load is increased. The extinguishing times are considerably reduced compared to the pure PA6 composite. The optimal load to achieve good results is 4 wt%, as higher values result in particle agglomeration and flame retardancy worsens. Comparing the UiO-66 samples, both activated and non-activated, it can be seen that at lower percentages, the activated sample performs better, while at higher values (4 wt%) the results are similar. Both samples achieve a V-2 classification in the UL-94 test, which would indicate that the washing and activation process is not necessary, thus resulting in a more sustainable process.

The best results obtained in the UL-94 test are achieved with the UiO-66/melamine sample. In this case, the higher the weight percentage, the shorter the extinguishing times. Both the composites with 4 and 7 wt% achieve a V-2 classification, although in the latter the times are slightly shorter. Melamine and UiO-66 act as flame retardants, while BDC helps to enhance compatibility with PA6.

An interesting future work could be to increase the percentage load of flame retardants to achieve a better classification in this burning test. Moreover, it is possible to study a homogeneous distribution of samples within the polymer in order to avoid agglomeration that worsens the results.

The LOI results have demonstrated an improvement in preventing the flammability of the PA6 composites, which is significantly enhanced for the UiO-66/melamine sample. Increasing the LOI from 22.4 % of PA6 to 23.2 % and 35.5 % for PA6 + activated UiO-66 and PA6 + UiO-66/melamine, respectively.

A flame retardant mechanism has been proposed for these materials, which involves: a) the formation of zirconium oxide, a refractory material that acts as an oxygen barrier to the interior and promotes soot formation: b) the adsorption of smoke and gases by UiO-66 prior to its degradation; c) the endothermic sublimation of melamine that adsorbs heat; d) the degradation of melamine, releasing ammonia that dilutes the combustion atmosphere.

Finally, it is worth noting that the novelty of this work lies in the fact that a new strategy has been proposed for the development of flame retardants based on MOF and melamine. These materials are synthesised with scalable procedures and in a single step, which makes the process more sustainable. Furthermore, these low loads flame retardants favourably modify the fire behaviour of polyamide 6, resulting in savings.

CRediT authorship contribution statement

Cristina Pina-Vidal: Writing – original draft, Visualization, Validation, Methodology, Investigation, Formal analysis, Conceptualization. **Víctor Berned-Samatán:** Investigation, Conceptualization. **Elena Piera:** Writing – original draft, Visualization, Resources, Project administration, Methodology, Funding acquisition, Conceptualization. **Miguel A. Caballero:** Resources, Project administration, Methodology, Funding acquisition, Conceptualization. **Carlos Téllez:** Writing – review & editing, Writing – original draft, Visualization, Validation,

Supervision, Resources, Project administration, Methodology, Funding acquisition, Conceptualization.

Declaration of competing interest

The authors declare the following financial interests/personal relationships which may be considered as potential competing interests: [The authors declare that this research work has been carried out within the LMP53_21 project that was funded by the Government of Aragon with co-funding of the company Nurel S.A. Elena Piera and Miguel Ángel Caballero were employed by the company Nurel S.A. The remaining authors declare that the research was conducted in the absence of any commercial or financial relationships that could be construed as a potential conflict of interest].

Acknowledgments

LMP53_21 project funded by the Department of Science, University and Knowledge Society of the Government of Aragon and co-financed by Nurel S.A. The University of Zaragoza for the use of the Servicio General de Apoyo a la Investigación-SAI and the use of instrumentation as well as the technical advice provided by the National Facility ELECMI ICTS, node "Laboratorio de Microscopias Avanzadas", at the Universidad de Zaragoza. The T68_23R group funded by Government of Aragon. Grant CEX2023-001286-S funded by MICIU/AEI/10.13039/501100011033.

Appendix A. Supplementary material

Supplementary data to this article can be found online at https://doi.org/10.1016/j.jiec.2024.10.026.

REFERENCES

[1] R. Zong, Y. Hu, N. Liu, S. Li, G. Liao, J. Appl. Polym. Sci. 104 (2007) 2297–2303, https://doi.org/10.1002/app.25691.
[2] P. Kiliaris, C.D. Papaspyrides, R. Pfaendner, Macromol. Mater. Eng. 293 (2008) 740–751, https://doi.org/10.1002/mame.200800111.
[3] J. Gao, Y. Wu, J. Li, X. Peng, D. Yin, H. Jin, S. Wang, J. Wang, X. Wang, M. Jin, Z. Yao, Compos. Part C: Open Access 9 (2022) 100297, https://doi.org/10.1016/j.jcomc.2022.100297.
[4] Y. Chen, Q. Wang, W. Yan, H. Tang, Polym. Degrad. Stab. 91 (2006) 2632–2643, https://doi.org/10.1016/j.polymdegradstab.2006.05.002.
[5] Z.Y. Wu, W. Xu, Y.C. Liu, J.K. Xia, Q.X. Wu, W.J. Xu, J. Appl. Polym. Sci. 113 (2009) 2109–2116, https://doi.org/10.1002/app.30022.
[6] N.L. Rosi, J. Eckert, M. Eddaoudi, D.T. Vodak, J. Kim, M. O'Keeffe, O.M. Yaghi, Science 300 (2003) 1127–1129, https://doi.org/10.1126/science.1083440.
[7] S. Ibrar, N. Zafar Ali, E.O. Ojegu, O.B. Odia, I.L. Ikhioya, I. Ahmad, J. Appl. Organomet. Chem. 3 (2023) 294–307, https://doi.org/10.48309/jaoc.2023.421600.1128.
[8] A. Sabetghadam, B. Seoane, D. Keskin, N. Duim, T. Rodenas, S. Shahid, S. Sorribas, C.L. Guillouzer, G. Clet, C. Tellez, M. Daturi, J. Coronas, F. Kapteijn, J. Gascon, Adv. Funct. Mater. 26 (2016) 3154–3163, https://doi.org/10.1002/adfm.201505352.
[9] R.Q. Zou, H. Sakurai, Q. Xu, Angew. Chem., Int. Ed. 45 (2006) 2542–2546, https://doi.org/10.1002/anie.200503923.
[10] A. Dhakshinamoorthy, A. Santiago-Portillo, A.M. Asiri, H. Garcia, ChemCatChem 11 (2019) 899–923, https://doi.org/10.1002/cctc.201801452.
[11] A. Dhakshinamoorthy, Z. Li, S. Yang, H. Garcia, Chem. Soc. Rev. 53 (2024) 3002–3035, https://doi.org/10.1039/D3CS00205E.
[12] A. Dhakshinamoorthy, S. Navalón, A. Primo, H. García, Angew. Chem., Int. Ed. 63 (2024) e202311241.
[13] R. Taghavi, S. Rostamnia, Chem. Methodol. 6 (2022) 639–648, https://doi.org/10.22034/chemm.2022.340599.1511.
[14] M.D. Allendorf, C.A. Bauer, R.K. Bhakta, R.J.T. Houk, Chem. Soc. Rev. 38 (2009) 1330, https://doi.org/10.1039/b802352m.
[15] A. Amiri, F. Ghaemi, B. Maleki, Microchim. Acta 186 (2019) 131, https://doi.org/10.1007/s00604-019-3246-7.
[16] P. Horcajada, C. Serre, G. Maurin, N.A. Ramsahye, F. Balas, M. Vallet-Regí, M. Sebban, F. Taulelle, G. Férey, J. Am. Chem. Soc. 130 (2008) 6774–6780, https://doi.org/10.1021/ja710973k.
[17] C. Pina-Vidal, V. Berned-Samatán, E. Piera, M.Á. Caballero, C. Téllez, Polymers 16 (2024) 637, https://doi.org/10.3390/polym16050637.
[18] M. Rafiul Hasan, A. Moriones, M. Malankowska, J. Coronas, Sep. Purif. Technol. 304 (2023) 122355, https://doi.org/10.1016/j.seppur.2022.122355.
[19] H. Nabipour, X. Wang, L. Song, Y. Hu, Composites, Part A 139 (2020) 106113, https://doi.org/10.1016/j.compositesa.2020.106113.
[20] P. Lyu, Y. Hou, J. Hu, Y. Liu, L. Zhao, C. Feng, Y. Ma, Q. Wang, R. Zhang, W. Huang, M. Ma, Polymers 14 (2022) 5279, https://doi.org/10.3390/polym14235279.
[21] X. Jin, X. Wu, Q. Liu, S. Sun, S. Cui, S. Zhang, C. Chen, Polym. Adv. Technol. 35 (2024) e6221.
[22] X.-L. Qi, D.-D. Zhou, J. Zhang, S. Hu, M. Haranczyk, D.-Y. Wang, A.C.S. Appl, Mater. Interf. 11 (2019) 20325–20332, https://doi.org/10.1021/acsami.9b02357.
[23] X. Shi, X. Dai, Y. Cao, J. Li, C. Huo, X. Wang, Ind. Eng. Chem. Res. 56 (2017) 3887–3894, https://doi.org/10.1021/acs.iecr.6b04204.
[24] X. Wang, S. Wang, W. Wang, H. Li, X. Liu, X. Gu, S. Bourbigot, Z. Wang, J. Sun, S. Zhang, Compos. Part B 183 (2020) 107568, https://doi.org/10.1016/j.compositesb.2019.107568.
[25] M. Ramezanzadeh, A. Tati, G. Bahlakeh, B. Ramezanzadeh, Chem. Eng. J. 408 (2021) 127366, https://doi.org/10.1016/j.cej.2020.127366.
[26] Y.-T. Pan, Z. Zhang, R. Yang, Compos. Part B 199 (2020) 108265, https://doi.org/10.1016/j.compositesb.2020.108265.
[27] W. Chen, Y. Jiang, R. Qiu, W. Xu, Y. Hou, Macromol. Res. 28 (2020) 42–50, https://doi.org/10.1007/s13233-019-7165-6.
[28] T. Sai, S. Ran, Z. Guo, Z. Fang, Compos. Part B 176 (2019) 107198, https://doi.org/10.1016/j.compositesb.2019.107198.
[29] X.G. Wang, P. Qi, S.J. Zhang, S.L. Jiang, Y.C. Li, J. Sun, B. Fei, X.Y. Gu, S. Zhang, Mater. Today Chem. 30 (2023) 101550, https://doi.org/10.1016/j.mtchem.2023.101550.
[30] X. Fan, F. Xin, W. Zhang, H. Liu, React. Funct. Polym. 174 (2022) 105260, https://doi.org/10.1016/j.reactfunctpolym.2022.105260.
[31] J. Zhang, Z. Li, Z.-B. Shao, L. Zhang, D.-Y. Wang, Chem. Eng. J. 400 (2020) 125942, https://doi.org/10.1016/j.cej.2020.125942.
[32] M. Pan, W. Chen, J. Dai, Z. Shu, H. Xue, J. Xu, H. Ou, 15280837221113361, J. Ind. Text. 52 (2022), https://doi.org/10.1177/15280837221113361.
[33] B.V. Lotsch, W. Schnick, Chem. Eur. J. 13 (2007) 4956–4968, https://doi.org/10.1002/chem.200601291.
[34] Y. Li, K. Liu, R. Xiao, Macromol. Res. 25 (2017) 779–785, https://doi.org/10.1007/s13233-017-5081-1.
[35] A.I. Balabanovich, Polym. Degrad. Stab. 84 (2004) 451–458, https://doi.org/10.1016/j.polymdegradstab.2003.12.003.
[36] C. Hoffendahl, G. Fontaine, S. Bourbigot, Polym. Degrad. Stab. 98 (2013) 1247–1255, https://doi.org/10.1016/j.polymdegradstab.2013.03.002.
[37] L. Xu, C. Lei, R. Xu, X. Zhang, J. Xu, Polym. Bull. 75 (2018) 2707–2727, https://doi.org/10.1007/s00289-017-2177-x.
[38] D. Liu, G. Cai, J. Wang, X. Tan, H. Lu, S. Zhang, Q. Dai, J. Appl. Polym. Sci. 131 (2014) 40254, https://doi.org/10.1002/app.40254.
[39] G. Yuan, Y. Yu, J. Li, D. Jiang, J. Gu, Y. Tang, H. Qiu, W. Xiong, N. Liu, J. Mol. Liq. 328 (2021) 115484, https://doi.org/10.1016/j.molliq.2021.115484.
[40] N. Yin, K. Wang, Y.a. Xia, Z. Li, Desalination 430 (2018) 120–127, https://doi.org/10.1016/j.desal.2017.12.057.
[41] R. Ghanbari, A. Marandi, E.N. Zare, J. Environ. Chem. Eng. 11 (2023) 109269, https://doi.org/10.1016/j.jece.2023.109269.
[42] ChemSketch, version 20222 1.2, Advanced Chemistry Development, Inc. (ACD/Labs), Toronto, ON, Canada, www.acdlabs.com.
[43] C.F. Macrae, I. Sovago, S.J. Cottrell, P.T.A. Galek, P. Mccabe, E. Pidcock, M. Platings, G.P. Shields, J.S. Stevens, M. Towler, P.A. Wood, J. Appl. Crystallogr. 53 (2020) 226–235, https://doi.org/10.1107/s1600576719014092.
[44] S. Øien, D. Wragg, H. Reinsch, S. Svelle, S. Bordiga, C. Lamberti, K.P. Lillerud, Cryst. Growth Des. 14 (2014) 5370–5372, https://doi.org/10.1021/cg501386j.
[45] B. Mayoral, E. Harkin-Jones, P.N. Khanam, M.A. Almaadeed, M. Ouederni, A. R. Hamilton, D. Sun, RSC Adv. 5 (2015) 52395–52409, https://doi.org/10.1039/c5ra08509h.
[46] S. Ding, X. Zeng, Chem. Phys. (2021), https://doi.org/10.48550/arXiv.2109.12435.
[47] M. Ermer, J. Mehler, B. Rosenberger, M. Fischer, P.S. Schulz, M. Hartmann, ChemistryOpen 10 (2021) 233–242, https://doi.org/10.1002/open.202000291.
[48] X. Chen, Y. Lyu, Z. Wang, X. Qiao, B.C. Gates, D. Yang, ACS Catal. 10 (2020) 2906–2914, https://doi.org/10.1021/acscatal.9b04905.
[49] M. Ermer, J. Mehler, M. Kriesten, Y.S. Avadhut, P.S. Schulz, M. Hartmann, Dalton Trans. 47 (2018) 14426–14430, https://doi.org/10.1039/c8dt02999g.
[50] C. Zou, S. Vagin, A. Kronast, B. Rieger, RSC Adv. 6 (2016) 102968–102971, https://doi.org/10.1039/c6ra23947a.
[51] G.E. Decker, Z. Stillman, L. Attia, C.A. Fromen, E.D. Bloch, Chem. Mater. 31 (2019) 4831–4839, https://doi.org/10.1021/acs.chemmater.9b01383.
[52] K.A. Milakin, S. Gupta, L. Kobera, A. Mahun, M. Konefał, O. Kočková, O. Taboubi, Z. Morávková, J.M. Chin, K. Allahyarli, P. Bober, A.C.S. Appl, Mater. Interf. 15 (2023) 23813–23823, https://doi.org/10.1021/acsami.3c03870.
[53] H.R. Abid, H. Tian, H.-M. Ang, M.O. Tade, C.E. Buckley, S. Wang, Chem. Eng. J. 187 (2012) 415–420, https://doi.org/10.1016/j.cej.2012.01.104.
[54] M.A. Rodrigues, J.d.S. Ribeiro, E.d.S. Costa, J.L.d. Miranda, H.C. Ferraz, Sep. Purif. Technol. 192 (2018) 491–500, https://doi.org/10.1016/j.seppur.2017.10.024.
[55] H. Zhu, S.-A. Xu, RSC Adv. 8 (2018) 17879–17887, https://doi.org/10.1039/C8RA01846D.
[56] D. Wang, X. Zhang, S. Luo, S. Li, Adv. Mater. Phys. Chem. 02 (2012) 63–67, https://doi.org/10.4236/ampc.2012.24b018.
[57] Y. Wang, K. Kretschmer, J. Zhang, A. Mondal, X. Guo, G. Wang, RSC Adv. 6 (2016) 57098–57102, https://doi.org/10.1039/C6RA11809G.
[58] C.A. Téllez S, E. Hollauer, M.A. Mondragon, V.M. Castaño, Spectrochim. Acta, Part A 57 (2001) 993–1007, https://doi.org/10.1016/S1386-1425(00)00428-5.

[59] M. Aghajanzadeh, M. Zamani, H. Molavi, H. Khieri Manjili, H. Danafar, A. Shojaei, J. Inorg. Organomet. Polym. Mater. 28 (2018) 177–186, https://doi.org/10.1007/s10904-017-0709-3.
[60] E. Piorkowska, G.C. Rutledge, Handbook of polymer crystallization, John Wiley & Sons, 2013.
[61] J. Huang, W. Ulrich, S. Schmauder, S. Geier, Comput. Mater. Sci. 50 (2011) 1315–1319, https://doi.org/10.1016/j.commatsci.2010.03.012.
[62] J. Sun, L. Qian, J. Li, Polymer 210 (2020) 122994, https://doi.org/10.1016/j.polymer.2020.122994.
[63] Y. Bai, Z.H. Han, H.Q. Li, C. Xu, Y.L. Xu, Z. Wang, C.H. Ding, J.F. Yang, Appl. Surf. Sci. 257 (2011) 7210–7216, https://doi.org/10.1016/j.apsusc.2011.03.092.
[64] H. Vahabi, F. Laoutid, M. Mehrpouya, M.R. Saeb, P. Dubois, Mater. Sci. Eng. R: Rep. 144 (2021) 100604, https://doi.org/10.1016/j.mser.2020.100604.
[65] J.F. Moulder, W.F. Stickle, P.E. Sobol, K.D. Bomben, Handbook of X-Ray Photoelectron Spectroscopy Physical Electronics Division, Eden Prairie, Minn., Perkin-Elmer Corporation, 1992.
[66] C. Shimasaki, N. Watanabe, K. Fukushima, S. Rengakuji, Y. Nakamura, S. Ono, T. Yoshimura, H. Morita, M. Takakura, A. Shiroishi, Polym. Degrad. Stab. 58 (1997) 171–180, https://doi.org/10.1016/S0141-3910(97)00043-8.
[67] K. Fang, J. Li, C. Ke, Q. Zhu, K. Tao, J. Zhu, Q. Yan, Polym. Eng. Sci. 51 (2011) 377–385, https://doi.org/10.1002/pen.21804.
[68] Y. Hu, S. Wang, Z. Ling, Y. Zhuang, Z. Chen, W. Fan, Macromol. Mater. Eng. 288 (2003) 272–276, https://doi.org/10.1002/mame.200390017.
[69] F. Sheng, X.Z. Tang, S. Zhang, X. Ding, Z.Z. Yu, Z. Qiu, Polym. Adv. Technol. 23 (2012) 137–142, https://doi.org/10.1002/pat.1833.
[70] K. Tamura, S. Ohyama, K. Umeyama, T. Kitazawa, A. Yamagishi, Appl. Clay Sci. 126 (2016) 107–112, https://doi.org/10.1016/j.clay.2016.02.027.
[71] X. Sun, C. Huang, Z. Chen, R. Zhou, J. Jiang, Polym. Test. 115 (2022) 107766, https://doi.org/10.1016/j.polymertesting.2022.107766.
[72] P. Lu, Z.-Y. Zhao, B.-R. Xu, Y.-M. Li, C. Deng, Y.-Z. Wang, Chem. Eng. J. 379 (2020) 122278, https://doi.org/10.1016/j.cej.2019.122278.
[73] Z. Zhang, M. Yang, K. Cai, Y. Chen, S. Liu, W. Liu, J. Liu, Materials 15 (2022) 813, https://doi.org/10.3390/ma15030813.